Experimental study of the influence of the relative humidity of leaves and their link to adhesion losses in the wheel-rail contact

Samy Guidoum, Pierrick Merino, Aurélien Saulot, Yves Berthier, Sylvain Hervieu

Mechanics & Industry **23**, 23 (2022)
© S. Guidoum et al., Published by EDP Sciences, 2022
https://doi.org/10.1051/meca/2022017

Mechanics & Industry

Available online at:
www.mechanics-industry.org

REGULAR ARTICLE

OPEN ACCESS

Experimental study of the influence of the relative humidity of leaves and their link to adhesion losses in the wheel-rail contact

Samy Guidoum[1,2,*], Pierrick Merino[1], Aurélien Saulot[1], Yves Berthier[1], and Sylvain Hervieu[2]

[1] Univ Lyon, INSA Lyon, CNRS, LaMCoS, UMR5259, 69621 Villeurbanne, France
[2] SNCF Réseau, Railway Division, 75010 Paris, France

Received: 16 February 2022 / Accepted: 25 May 2022

Abstract. Every autumn, low levels of wheel–rail contact adhesion caused by leaves on the railhead surface are reported by train drivers. These incidents cause problems for the safety and regularity of rail traffic and occur predominantly at the beginning and end of the day when high humidity levels are achieved. At those moments the air temperature reaches the dew point temperature creating moisture on the railhead and oxides which react chemically with dead leaves found on the railhead surface. This article presents the results of a test campaign performed on a ring-on-disc tribometer with the aim of reproducing and studying the development of a loss of adhesion at an imposed slip rate. This type of tribometer enables a realistic approximation of the tribological circuit of a rail–wheel contact. Several samples of pollution responsible for adhesion losses were collected on the French railway network during fall and reproduced in a laboratory on a tribometer under imposed relative humidity and slip conditions. The results indicate the presence of reproducible phenomena modulated by variations in hygrometry and imposed slip rates. The decrease in hygrometry of the external third bodies introduced into the contact is at the origin of the generation of debris from the first bodies in contact. This presence of wear debris is reflected by an increase of the power dissipated by friction. Conversely, increasing the hygrometry decreases the ability of the third body to raise adhesion levels on contact and reduces the generation of debris from the first bodies. The results obtained from the analysis of the force and power quantities related to the contact reproduced in the laboratory allow the authors to confirm that the presence of water has a significant effect on the mechanical and physico-chemical evolution of the adhesion of a rail–wheel contact polluted by a third external (leaf-like) body.

Keywords: Wheel–rail contact / adhesion / third body layer / leaves / tribology

1 Introduction

The use of train transportation systems is becoming increasingly popular each year in France and are probably the most sustainable means of mass transportation available today. In autumn, security and regularity issues concern several rail networks because of the mixture of contaminants on the head of rails. Therefore, when a braking train rolls on polluted rails, the braking forces cannot be fully transmitted due to the reduction of the contact's adhesion and will lead the railway traffic to miss a signal or a station. In addition, when an accelerating train rolls on polluted rails, the traction forces generated by the engines to the contact will, once again, not be fully transmitted and will be the source of wheel-slipping events. This type of incident can damage both wheels and rails (Fig. 1).

Since 2016, internal studies focusing on wheel–rail adhesion performed by the French National Railway Company (SNCF) have highlighted the main sources of pollution at the origin of wheel slip (occurring during acceleration) and wheel slide (occurring during braking) incidents in the autumn. The majority of the main adhesion loss incidents (62%) were due to the presence of crushed dead leaves by trains on the head of the rail in an atmosphere with high relative humidity (RH) levels and low temperatures. The same points were also shown through studies [1,2] of key performance indicators obtained from Great–Britain railway networks associated to wheel-rail adhesion losses (such as station overruns and signals passed at danger). These incidents were both linked to the presence of autumn leaves and temperature fluctuation around the dew point for about 50% of the total number of incidents retained by these authors.

When an adhesion-loss incident due to the presence of crushed leaves in the contact occurs, an adhesive black layer on a rail surface is created and leads to the loss of both the electrical and mechanical contact. The two first solids/bodies initially in contact, the wheel and rail, are separated from each other by the presence of another

* e-mail: samy.guidoum@insa-lyon.fr

Fig. 1. Rail damage due to wheel-slip event in France; the squared area is the result of damage to the rails caused by train wheels.

body (layer of leaves, sand, grease). This idea is part of a conceptual tool, initially introduced by Godet [3]. Two solids in contact called first bodies are separated by a third one called a third body and linked by a "mechanism". It includes the contact stresses, stiffnesses, damping, and the inertia of the two first bodies (Fig. 2a). For a wheel–rail contact, the third body can be from the two first bodies (wear of wheels and rails) or from an external source (ejection of sand particles (Fig. 2b), braking shoe particles, water, or even leaves).

The effect of falling leaves from a chemical aspect was studied by Ishizaka [2] and Cann [5]. They showed that five main chemicals could drive the creation of this layer : lignin ($C_9H_{10}O_2$), pectin ($C_6H_{10}O_7$), cellulose ($C_6H_{10}O_5$), water (H_2O), and iron (Fe). These chemical components appear when the plant cell walls start degrading (Fig. 3).

More recently, Bringel [7] explained the main chemical mechanisms at the origin of the creation of the black layer previously mentioned and its bonding to the rail. Several chemical reactions between dead leaves and surface elements (mainly iron oxides and carbon) of a rail were shown to be at the root of the bonding mechanism. A first chemical reaction occurs when an acidic pH level generated by the degradation of the walls of the dead leaves (Fig. 3) is obtained and put in contact with water (condensation, rain, etc.).

After a short period, usually a few hours, the components of a degraded dead leaf (mainly lignin and cellulose) react with the iron in the rail steel to form Fe^{3+} and Fe^{2+} ions. The acidification of the surface of a rail with degraded dead leaves due to water tends to oxidize and dissolve the Fe^{3+} ions in the first 15 µm of a wet rail surface. Associated with this dissolution, the biopolymers formed are adsorbed into the porosities of the steel, created by the dissolution of the iron, and increase its adhesion to the rails. A black and adhesive layer of various thickness appears on the rail surface. The chemical composition of this black layer was also studied by Watson et al. [8] and reveals the presence of iron tannate produced by a reaction between poly-phenols and dissolved iron [9]. The results of this last study showed strong evidence that tannins alone can cause low adhesion while other chemicals in the leaf extracts used to performed adhesion tests by these authors cannot. Therefore, this type of chemical reaction found here can be linked to low adhesion for the wheel-rail contact.

The color change of a dead leaf is also an indicator of the physico-chemical transformations occurring in the life of a polluted wheel–leaves–rail contact. As an example, the color changes of leaves during fall results from the decrease of chlorophyll production in the cells of the leaves. In the same way, the change from a light brown to a black color of a mixture of water, dead leaves, and steel is synonymous with a reaction linked to the formation of a complex between lignin and iron in an aqueous environment [10]. As a final example, rust is usually formed by the reaction of iron, oxygen, and water or air moisture and can be found on the surface of corroded steel. The presence of a red-brown color is synonymous with an increase in the degree of oxidation of iron hydroxide. Therefore, the observation of color changes of a third body can be used as a qualitative means to determine the occurrence of physicochemical reactions upon contact.

These different chemical reactions occur without mechanical stresses. The passage of the wheel of a train onto these chemical complexes will transform the cementite present in the bulk of a rail into graphite, which can have a high resistivity and be the source of the loss of the electrical contact of a train wheel and its rail [11].

Thus, using these works and the observations made under both real conditions and laboratory conditions (controlled ambient temperature and RH), the presence of water in a liquid form combined with the presence of dead leaves on rails are *sine qua non* for low adhesion levels. However, very few studies have examined the effect of the hygrometry level of dead leaves creating a black layer being responsible for adhesion losses.

This work presents the experimental reproduction of one type of rail pollution with various levels of RH and wheel slip rates. The aim of this work was to study the effect of these two parameters on wheel–rail adhesion. To understand these phenomena from a mechanical perspective, adhesion tests with plane leaf samples were performed using on a novel test bench reproducing the rolling contact conditions [12] called Triboring. The leaf species used were considered an artificial third body introduced in the tribometer's contact. An analysis of the mechanical parameters (forces, torque, etc.) and surface observations of the different parts of the bench in contact was performed using optical and scanning electron microscopy with the aim of explaining the evolution of wheel-rail adhesion under various conditions.

The elements presented in this article can be positioned in relation to the recent work of Ishizaka [13], which mainly focused on studying the physico-chemical reactions involved in the transformation of dead leaves in connection with the loss of adhesion of a train. Spectroscopic analyses (i.e., the study of the interaction between matter and electromagnetic radiation as a function of the wavelength or frequency of the radiation) such as Fourier-transform infrared (FTIR) spectroscopy, Raman spectroscopy, X-ray photoelectron spectroscopy (XPS), and energy-dispersive

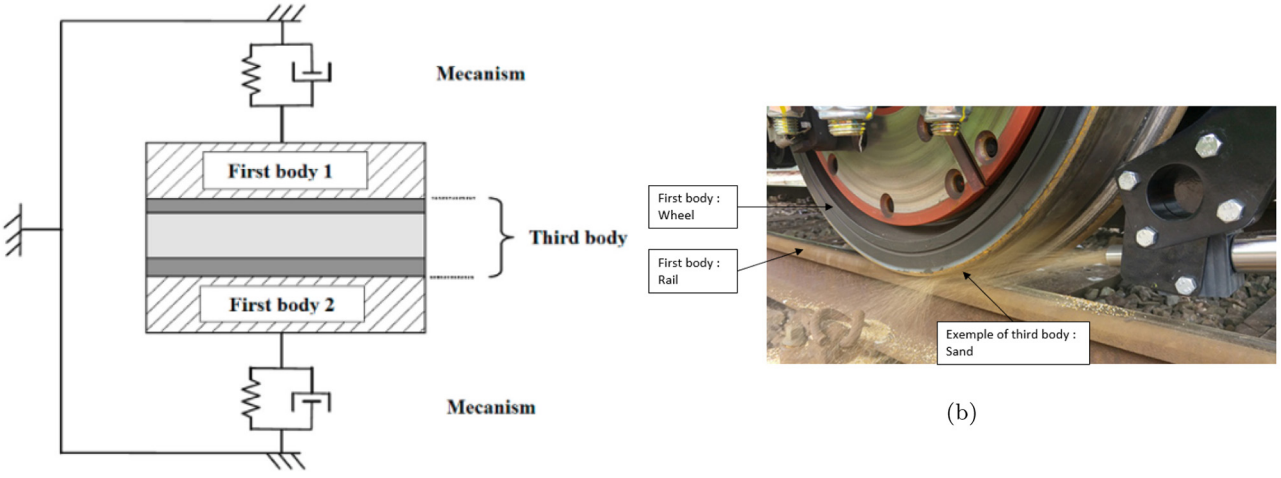

(a) (b)

Fig. 2. (a) The tribological triplet by Godet and Berthier [3,4], (b) application to a sanding system for the wheel–rail contact.

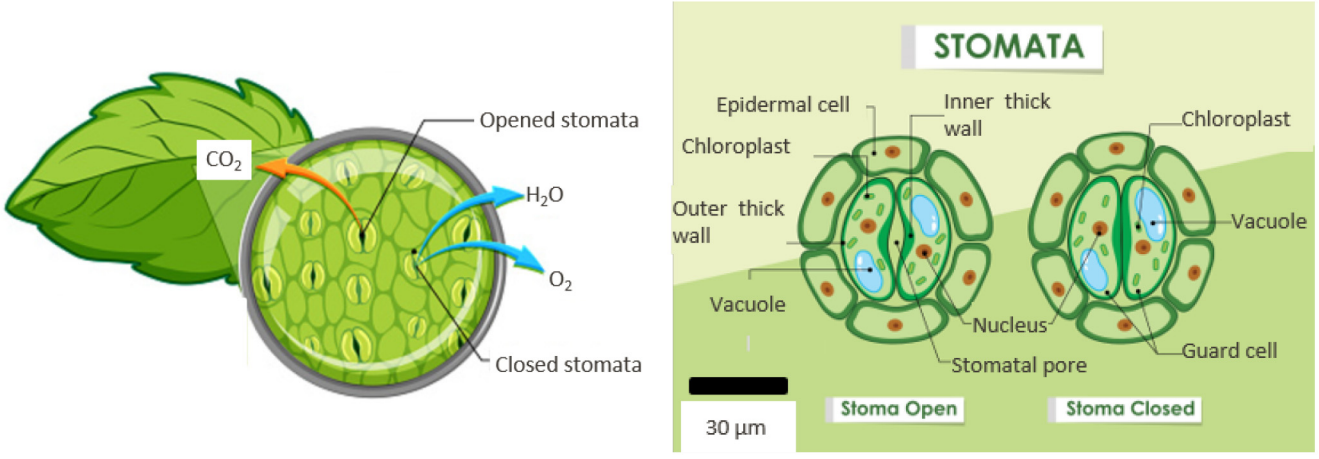

(a) (b)

Fig. 3. (a) Leaf stomata, (b) schematic of the stomata [6].

X-ray spectroscopy (EDS) were performed after grinding and drying dead leaves in aqueous solution. The structure of the leaves was thus modified and not fully representative of real conditions. Other analyses were also conducted after experiments performed using a bi-disc tribometer (reproducing a wheel–rail contact at a 1/24th scale). The advantage of this type of tribometer is that cyclic tests can be performed under imposed conditions. However, its use increases the wear flow of leaves generated on the parts in contact and accentuates the recirculation flows of the third bodies formed.

In this study, the work was performed using plane leaves that were not grinded. Their structures (both mechanical and physico-chemical) were therefore not changed and could be compared to those of crushed leaves commonly found on the surface of a rail.

As previously validated in a recent study [12], a ring-on-disc tribometer was also used to reproduce the wheel–rail contact (at a 1/16th scale) and its main mechanical parameters (contact pressure, slip rate, etc.). The tribometer's contact kinematics were also closer to those of a wheel–rail contact. However, unlike for the use of a bi-disc tribometer, a ring-on-disc tribometer drastically decreases the recirculation flow of the third bodies. It can also generate lateral material flows.

The aim of this work is therefore to study the adhesion of a wheel–rail contact reproduced on a tribometer at several slip rates and RH levels of an organic external third body.

2 Material and methods

2.1 Definition of adhesion for the wheel–rail contact community

For a tribologist, adhesion is linked to the force needed to separate two surfaces put in contact from each other.

The notion of adhesion is also used to describe how coatings are bonded to a substrate. For the wheel–rail research community, this term is linked to the description of the evolution of the tangential force resulting from this type of contact. Therefore, the words "adhesion losses" will be used to describe the results of the decrease of the tangential forces correlated to the rolling tests performed with a tribometer reproducing a wheel–rail contact. The main variable associated with these tests will be linked to a computed "friction factor" defined as the measured tangential force over the normal one (Eq. (3)). Therefore, due to the fact that the solids in motion in this study are either in rolling or rolling and sliding conditions, the use of a classical "friction coefficient" to describe adhesions losses of a wheel-rail contact is not appropriate. Indeed, the term "friction coefficient" is mainly referred to sliding condition or in incipient relative motion (static friction coefficient) which is not the case for the study presented in this article.

2.2 Experiments details

2.2.1 Management of the RH

Ishizaka [2] highlighted that the most dangerous adhesion loss events mostly occur in the early morning (between 6 am and 9 am) in the UK. In France, during this time period, the RH of the air can be higher than 85%. This RH level is recorded where there is light rain or dew. This author also showed that adhesion losses due to the presence of dead leaves on the rails also occur during other times of day. They occur when a train rolls onto a polluted rail with a slip rate different than 0% at the middle or end of the day. During these two time periods, in October and November, the RH of the air is usually near 50% and lower than 35% in France. These incidents occur with a lower impact than those linked to a high RH in the morning. Smaller distances are needed to achieve commercial speed. Few studies [14–17] have focused on the effect of the RH on the adhesion of the wheel–rail contact, and they all showed that the RH of an environment has a major effect on the wheel–rail adhesion.

Therefore, to be representative of the conditions studied in the main articles related to this parameter [2,14], three levels of RH of the fallen plane leaves were selected ($RH \leq 35\%$, $RH \approx 50\%$, and $RH \geq 85\%$) during tribometer testing. The test conditions are summarized in Table 1. When RH is below 35%, the external third body is considered "dry" and is representative of mid-afternoon conditions. When RH is approximately equal to 50%, the external third body is considered "intermediate" and is representative of end-of-morning or end-of-afternoon conditions. Finally, when RH is higher than 85%, the external third body is considered "wet" and is representative of early morning and/or early evening conditions.

The RH of the third body used is controlled using a hygrometer with a probe, allowing the values to be directly read with a precision of ±0.1%. To obtain dry plane leaves, with RH below 35%, the leaves are placed in an air-tight box containing a desiccant to lower the moisture content from 50% to under 35%. For intermediary conditions, plane leaves are left in open air with approximately $50 \pm 5\%$. of hygrometry and at room temperature ($20\,°C \pm 5°$.) (see Fig. 4). To achieve wet conditions ($RH \geq 85\%$), a dozen of plane tree leaves were soaked with 2 L of distilled water (pH of 5.8). This initiated one of the chemical reactions (degradation of the molecules of cellulose, lignin, and hemicellulose composing the walls of the dead leaves due to an acidic pH level) [7]. This type of leaf was identified by the French National Railway Company (SNCF) to be one of the most preponderant species found after train adhesion loss.

Table 1. Summary of common adhesion test conditions.

Standard test conditions	
Ring steel	R260
Disc steel	ER7
Disc radius	35 ± 0.1 mm
Disc radius of curvature	70 ± 0.1 mm
Ring linear speed	1.3 m s^{-1}
Theoretical Hertzian pressure	1 GPa
Normal force	1 kN
Acquisition frequency	2000 Hz
Disc rotational speed ω_d	41.3 rd s^{-1}
Ring rotational speed ω_r	1.4 rd s^{-1}

2.2.2 Test bench and associated measured data

To reproduce the rolling-contact conditions, a novel test bench called Triboring (Fig. 5) was developed [12]. It consists of a small disc of 70-mm diameter (representing the wheel), rotating on a horizontal circular ring of 2-m diameter (the rail).

The rail part consists of a 2-m-diameter forged ring of R260 steel bloom with a rectangular section of 75 mm × 50 mm. The microstructure and composition of the alloy can be found in [18] (Tab. 2). The thermal process applied during the ring-rolling forging leads to a similar microstructure of R260 rails [19] (similar hardness, phases, and grain size), with a fully pearlitic microstructure. The wheel part is a convex disc manufactured from an ER7 head wheel (Ra 0.8 µm) and mounted on an electric motor.

Both the rotational speeds of the ring and the disc are measured with two incremental displacement encoders (8192 divisions for the disc, 3600 divisions for the ring). The measurements of the normal and tangential forces near the contact are performed using four specifically designed three-axis strain gauges. Each gauge can measure forces with a measurement range of ±3 kN for two directions and ±1 kN for the third one. The motor torque applied to the shaft where the disc is mounted was measured. Each experiment was filmed to observe and correlate the evolution of the disc and the ring surfaces with the data measured.

The measurement of the rotational speeds of the disc and ring enabled to impose a slip rate on the contact with a precision of less than 0.05% [19].

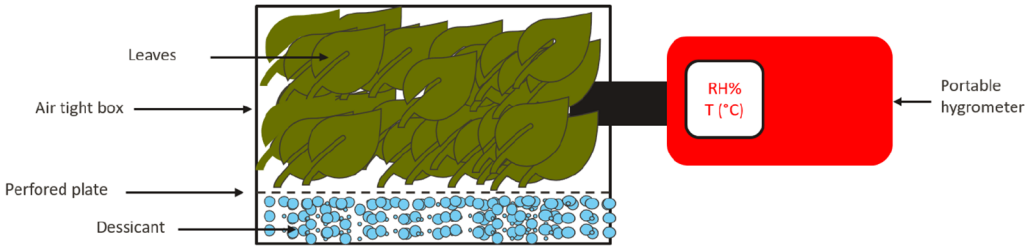

Fig. 4. Illustration of apparatus used to measure RH of the third body.

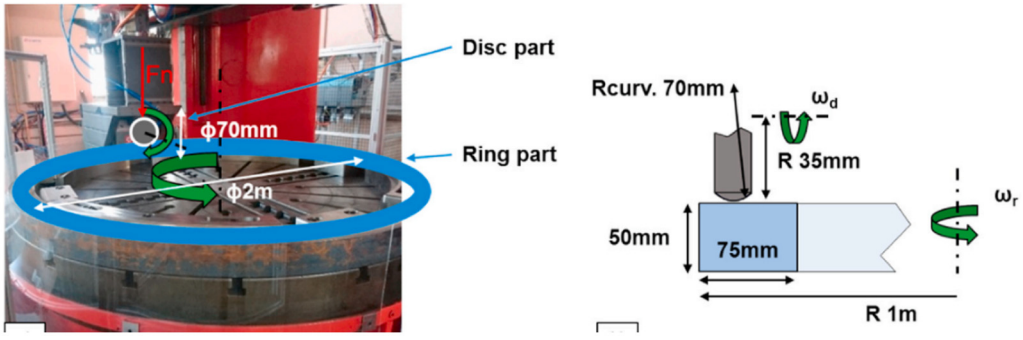

Fig. 5. Triboring test bench, a disc in rotation on a circular rail (the ring) [12].

Table 2. Chemical composition of R260 Steel [18] and ER7 steel [20], (weight %).

Chemical composition (weight %)												
	C	Si	Mn	P	S	Cr	Al	Cu	Mo	Ni	V	Cr+Mo+Ni
R260 Steel	0.62–0.8	0.15–0.58	0.7–1.20	⩽0.025	⩽0.025	⩽0.15	⩽0.004					
ER7 Steel	0.52	0.40	0.80	0.020	0.020	0.30		0.30	0.08	0.30	0.06	0.50

2.2.3 Management of the slip rate

Considering the radius of the disc and its position with respect to the center of the ring, a factor between the rotational speed of the disc and the ring was defined to apply a slip rate at the contact. A static vertical load was applied on the disc in order to obtain the desired theoretical pressure at the contact. The slip rate was calculated using:

$$\gamma = \frac{V_d - V_r}{(V_d + V_r)} = \frac{R_d\omega_d - R_r\omega_r}{R_d\omega_d + R_r\omega_r} \quad (1)$$

Here, V_d and V_r are the speed of the disc, imposed by a motor torque, and the speed of the ring at the point of contact; ω_d and ω_r are their rotational speeds, respectively; R_d is the radius of the disc; and R_r is the distance between the center of contact and the center of the ring (Sect. 2.2.6). The ER7 steel grade wheel (represented by the disc) is driven by a control command designed to maintain a user-defined constant slip rate value related to the ring speed.

The trains in circulation are mostly equipped with anti-slip control software, avoiding high sliding conditions in acceleration and braking areas. For example and reference, the slip threshold below which the anti-slip software is inactive is lower than 2% in Paris Public Transportation [21]. Therefore, to study the effect of this parameter on wheel–rail adhesion without any effect of the anti-slip software, two types of experiments using the Triboring tribometer were performed. The first one consisted of using a slip rate close to 0%, which is equivalent to a pure rolling condition. The second one consisted of reproducing a movement of acceleration by using a slip rate higher than 0.5%. Typical values of this factor found in the literature are 0.5%, 1%, and 1.5% [12,22,23]. A slip rate threshold of 1.5% was selected to be able to compare the results (friction factors curves) obtained with those of other authors. Beyond these values, if the system control takes no measure regarding the regulation of the slip rate, the wheels will start to slip excessively and will not be able to transmit all the forces linked to the movement but will create rail or wheel defects.

The adhesion tests described and explained in this paper were therefore performed with these three slip rates imposed on the test bench. The test conditions are described in the Section 2.2.6.

2.2.4 Methods of analysis

Rolling tests performed with the Triboring tribometer were analyzed numerically using classical mechanical quantities (forces, motor torque, friction factor) and measured as close as possible to the contact in Section 2.2. Samples of the third body were collected from the surface of the disc and ring and observed using optical microscopy

Table 3. Comparison of elements after EDS analysis performed on several samples (on site and laboratory).

List of elements detected by EDS	On-site sample	Tribometer test (RH: 85%, Slip rate: 1%)
C	x	x
O	x	x
Fe	x	x
Si	x	x
K	x	x
Mg	x	-

(Keyence VHX-2000F). Scanning electron microscopy (SEM) was also used (Quanta 200 MKII, Quanta FEG 650 with energy-dispersive spectrometry (EDS) probe). The samples of the third body were observed using a secondary-electron detector (SE) and a back-scattered electron (BSE) detector with an acceleration voltage in the range of 15–20 kV.

As an example, an SEM image in SE mode coupled with an EDS analysis of a sample taken on site are shown in Figure 6. In comparison, a test performed with a slip rate equal to 1% and a residual RH of the third body higher than 85% is shown in Figure 7.

Figures 6 and 7 compare the presence of chemical elements in two samples from two different areas (on the surface of a rail and in the laboratory). In both cases, the energy rays allow identification of organic elements from plants but also certain elements from R260 steel parts (Tab. 2) such as iron, sulfur, and silica. The authors would also like to point out the fact that carbon is present in all the elements in contact (rail, wheel, third organic body) during the tests carried out, therefore, as EDS analysis is not used to carry out quantitative studies, the use of a carbon support is not a concern for this study.

This tendency (also found in other analyses) allows the validity of the reproduction of a type of third body linked to adhesion issues to be justified. This is explained by the presence of the same elements found through several EDS analyses performed on site samples and laboratory samples. These elements are summarized in Table 3. These analyses can also be extended by using chemical spectroscopy (as a further work).

2.2.5 Test results processing

When conducting adhesion tests for a dry wheel–rail contact, the use of the friction factor (Eq. (3)) provides an understanding of how the normal and tangential forces evolve within the contact. However, the introduction of an external third body in the tribological triplet studied here (disc, ring, and tribometer) demands further information. Indeed, the use of the friction factor alone does not allow the effect of the addition of matter in a contact to be described and should be complemented by the use of an energy quantity.

From an energy viewpoint, variations of the friction factor result in power dissipation by the contact. The latter can be linked to the variations of the morphology of the third bodies involved. From a tribological viewpoint, the power dissipated by friction (P_f, Eq. (2)) helps to identify the conditions necessary for a given third body to be solicited and be able to dissipate a maximum of energy by the contact and make a train move.

Indeed, the application of different slip rates and RH (for a wheel–rail contact polluted by leaves) modifies the way in which the power dissipated by friction by the contact will be mobilized through the tangential forces. Thus, correlating the power dissipated by friction and the friction factor can help to identify a threshold beyond which it will no longer be possible to solicit a third body from an energy and mechanical viewpoint.

In other words, conducting a parametric study linking the adhesion of a rail-wheel contact reproduced on the Triboring tribometer to variations in the slip rate and relative humidity of the third bodies is carried out through the analysis of a mechanical quantity (friction factor, μ Eq. (3)) and an energy quantity (the power dissipated by friction, P_f, Eq. (2)).

The coupled use of these two quantities allows the identification of conditions associated with the application of a slip rate and a change in relative humidity for which the power dissipated by friction will be maximum and resulting in a high friction factor (the two quantities are calculated from measurements of tangential forces). These data depend mainly on the morphology of the third bodies formed during experiments carried out for a range of RH and slip rates affecting the measured tangential forces. The application of a non-zero slip rate to the contact thereby provides the opportunity to act upon the third bodies formed from a mechanical point of view (analysable through the variations in forces measured as close to the contact as possible) but also from an energy point of view (analysable through the variations in power dissipated by friction).

The radii of the parts in contact as well as their respective speeds of rotation were measured. This data enabled computation of P_f. This quantity was calculated using the following equation:

$$P_f = |F_t * (V_d - V_r)| = |F_t * (R_d\omega_d - R_r\omega_r)| \quad (2)$$

The equation defining the power dissipated by friction is only valid for rolling conditions with sliding and does not consider the friction associated with pure rolling conditions combined with plastic deformation of solids and adhesion phenomena. However, the most safety critical adhesion losses of a train are encountered in the railway industry during acceleration and braking [24]. Therefore, the use of the equation defined here is appropriate for the

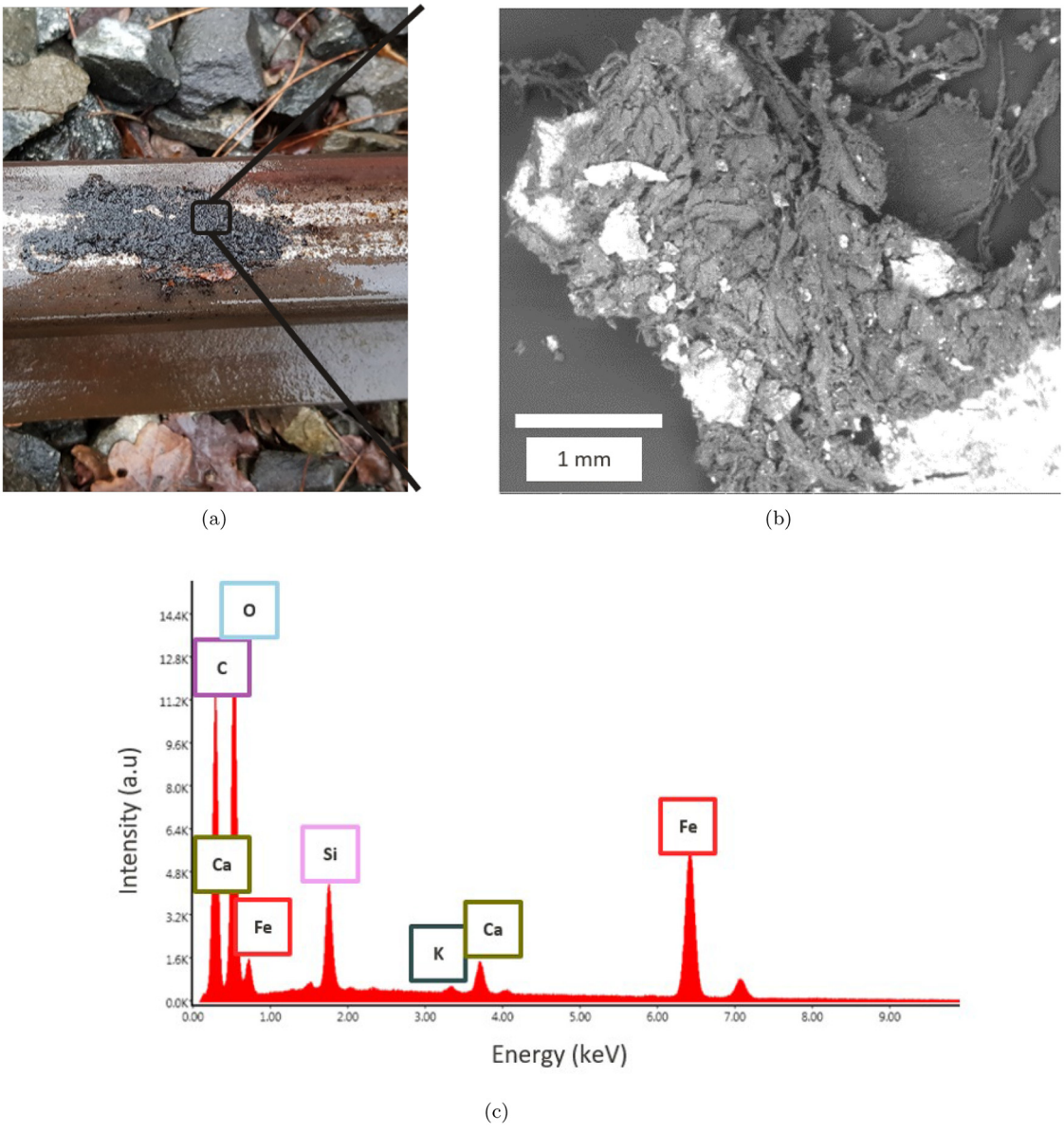

Fig. 6. (a) Macroscopic image of an on-site third body responsible for adhesion losses. (b) SEM image of the sample (BSE detector), (c) EDS spectrum of the sample observed (b). The elements found correspond to plant residues.

laboratory study of the adhesion of the wheel-rail contact in the presence of a non-zero slip rate in order to be able to come closer to the study of an industrial phenomenon.

The friction factor μ was also obtained using the ratio of the tangential and normal forces measured near the contact:

$$\mu = F_t/F_n \tag{3}$$

Here, V_d, V_r , ω_d, ω_r, R_d, R_r defined in Table 1 and Δi, the duration of the data acquisition, and a frequency of 2000 Hz were used. N is the number of points measured during a test. All the results measured were averaged using a moving mean with a period of approximately 4.4 s. This time (see also Tab. 1) corresponds to one revolution of the ring and allows the signals from high-frequency perturbations to be cleared.

The use of two cameras (visible spectrum, resolution: 1920×1080) enables monitoring of the evolution of the morphology as well as the color of the third bodies on the surface of the parts in contact. As mentioned in Section 1, the change in color of the third bodies signifies physico-chemical transformations and is also one of the criteria used to describe and understand the process of loss and recovery of adhesion of the contact studied.

2.2.6 Test conditions and associated campaigns

Adhesion tests are performed with common wheel–rail contact conditions (material properties, radii of curvature, normal force applied) viewable in Table 1. For these

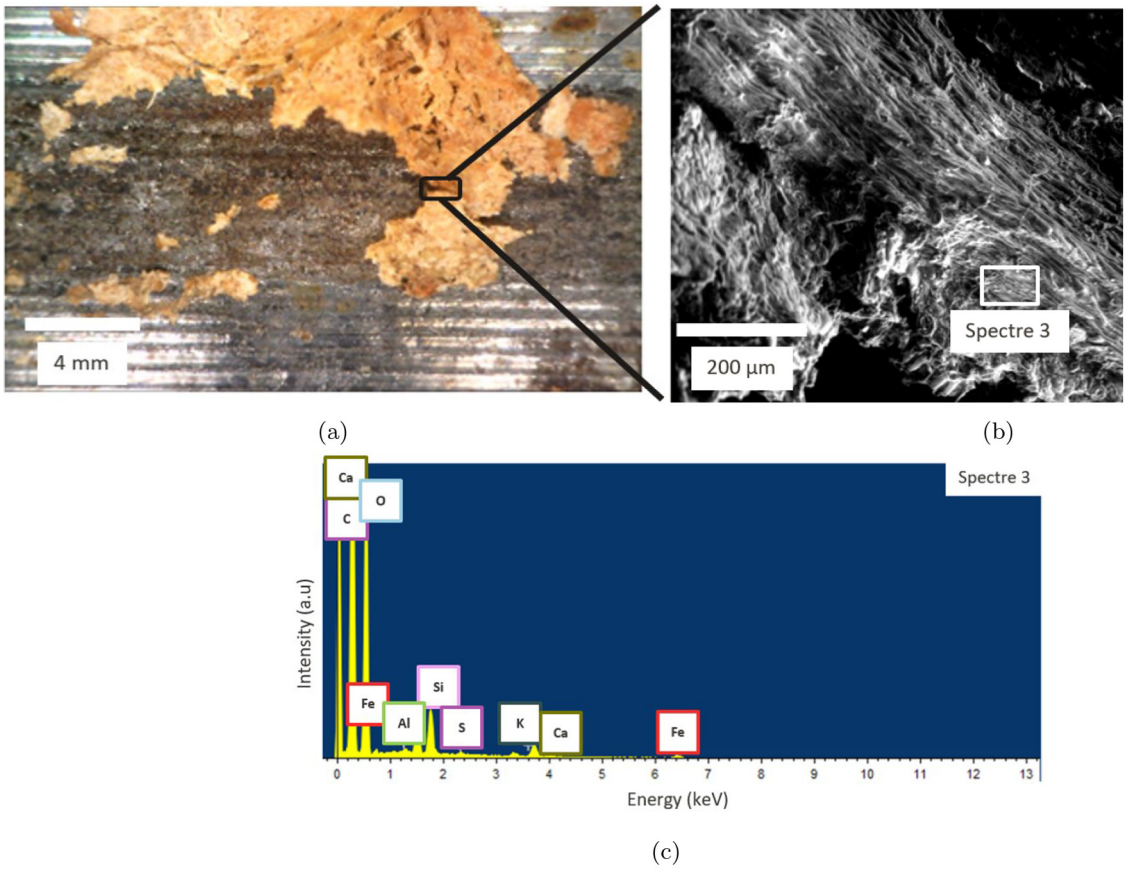

Fig. 7. (a) Macroscopic image of a laboratory-reproduced third body taken after a test (RH: 85%, Slip rate: 1%) on the Triboring tribometer. (b) SEM image of the sample (BSE detector), (c) EDS spectrum of the sample (b). The elements found correspond to plant residues and are similar to the one found in Figure 6.

conditions, the theoretical Hertz contact dimensions (half width and length) are 0.55 mm (longitudinal direction) and 0.86 mm (transverse direction). For all the tests, the ring rotation speed was set to 13.5 rpm (equivalent to a linear speed of 1.3 $m\,s^{-1}$), and the theoretical Hertzian pressure was 1 GPa (equivalent to a normal force of 1 kN in the present configuration).

With a linear ring speed of 1.3 $m\,s^{-1}$, the acquisition frequency of 2000 Hz enabled the collection of 366 measurements along the disc's circumference. The linear speeds in Table 1 depend of the ring radius.

The first series of tests were references tests performed without any artificial third body introduced in the contact but with four slip rates (0%, 0.5%, 1%, 1.5%). The experimental friction factor was computed from the ratio of the longitudinal and normal measured contact forces and is the main parameter used to have reference adhesion values.

The second series of tests were performed with the introduction of an artificial third body and were analyzed in a similar manner. The third body used was positioned over an area of length equal to one-wheel perimeter (approximately 210 mm). This zone is called "Area A" and has the aim of reproducing the pollution of one wheel on its perimeter. Figure 8 highlights this area.

3 Results

To the author's knowledge, no other adhesion tests involving an external third body have been performed on a disc-on-ring tribometer. Therefore, the objective of this section is to present the main results of the friction tests performed on the Triboring tribometer (Tab. 4). A proof of repeatability of the test is provided in Sections 3.1.1 and 3.1.2. The results of the test campaigns performed without the introduction of an external third body are presented in Section 3.1.3, and those done with the introduction of an external third body are presented in Section 3.1.4. The same data are described with energy values in Section 3.2 to highlight the links between RH and slip rate in determining the capability of a third body to modulate friction through power dissipation.

3.1 Adhesion tests

The objective of this section is to provide evidence related to the repeatability of the tests described in Table 4. All the test conditions were reproduced at least four times to enable calculation of the average values and standard deviations. The Figures 9 and 10 justify the repeatability of the different tests performed using two examples.

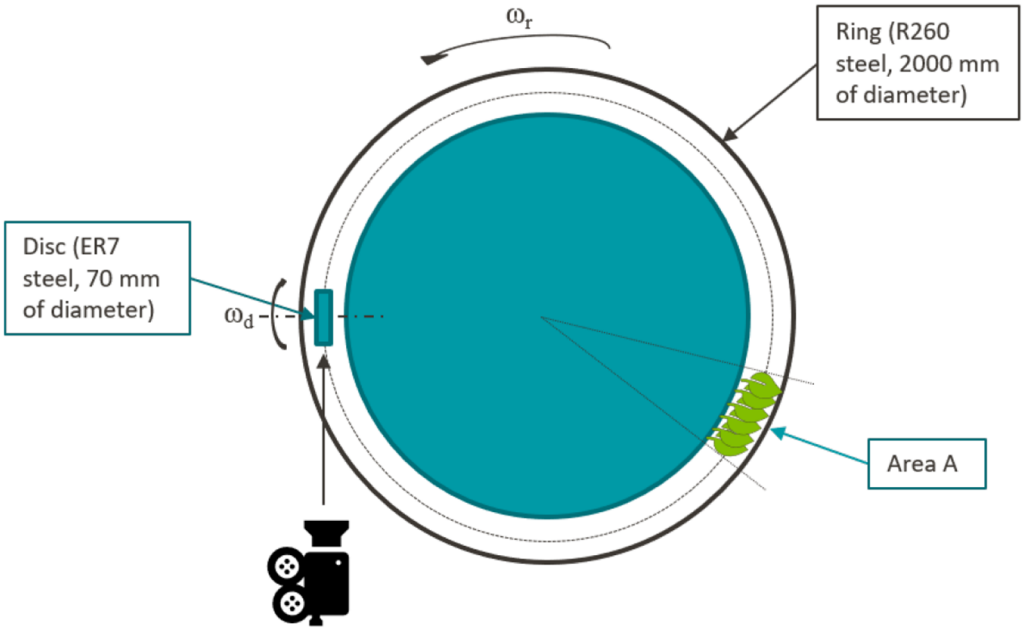

Fig. 8. Illustration of placement of leaves used during the tests reported in Table 4.

Table 4. Summary of test conditions.

Standard test conditions			
	RH of the third body		
Slip rate	[30; 35%]	[45; 55%]	⩽ 85%
0%	x	x	x
0.5%	x	x	x
1%	x	x	x
1.5%	x	x	x

3.1.1 Reproducibility of results without leaves

The repeatability of the data obtained after several test campaigns performed by Merino [12] with a corroded ring and R260 steel grade discs on the disc-on-ring tribometer used to study wheel–rail adhesion is justified in Figure 9. A friction factor $\mu = 0.2 \pm 0.0053$ was obtained after four tests were conducted under the same conditions. The aim of this study was to understand the mechanism of creation of a mechanical white etching layer responsible for rail defects.

The Triboring tribometer enabled repeatable friction results to be obtained related to the measurement of stable values on average, after post-processing with a measurement uncertainty below 10%. The tests performed without leaves but with an initially corroded ring and R260 steel grade discs permit the obtainment of a similar friction factor to the one obtained with other types of tribometer. The majority of the tests carried out in laboratory with rolling and sliding conditions to characterise the adhesion of the wheel-rail contact are performed using a twin disc tribometer [24]. This type of tribometer allows the reproduction of rolling and sliding conditions as does the Triboring tribometer. When comparing the friction factors for comparable tests conditions, similar values are obtained for both types of tribometers. As an example,

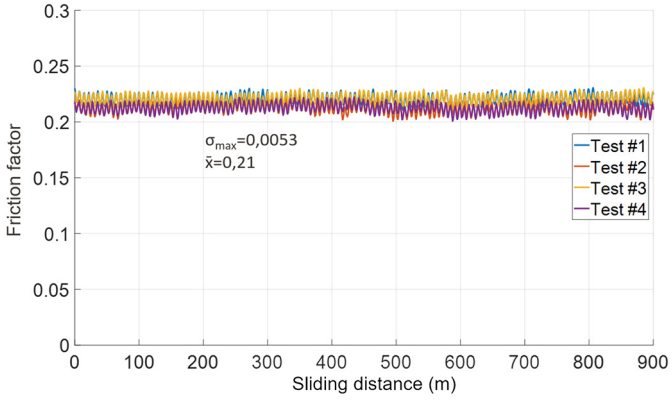

Fig. 9. Repeatability of a series of tests performed under a slip rate of 0.5% with an R260 disc and ring, average: 0.21, maximum standard deviation: 0.0053.

the tests performed by Gallardo-Hernandez and Lewis [25] on a twin disc tribometer with a slip rate of 0.5% and a contact pressure of 1500 MPa allow these authors to measure a friction factor close to 0.25 on average (vs 0.21 on the Triboring tribometer, with an R260 disc and ring).

3.1.2 Reproducibility of results with leaves

The objective of this section is to provide evidence related to the repeatability of the tests performed with leaves and mentioned in Table 4. The results are presented in Figure 10.

In Figure 10, the difference between the friction factor values can be explained by variations of the ambient temperature when the tests were performed. Tests #1 and #2 occurred in winter with an ambient temperature of 15 °C and a RH of 51%. Test #3 was conducted in the summer with an ambient temperature of 25 °C and a RH

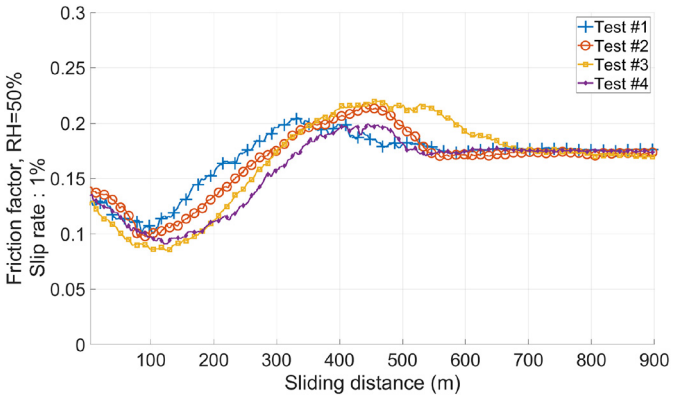

Fig. 10. Repeatability of a series of tests performed with leaves under a slip rate of 1% and a RH of 50%, average: 0.17, and maximum standard deviation: 0.031.

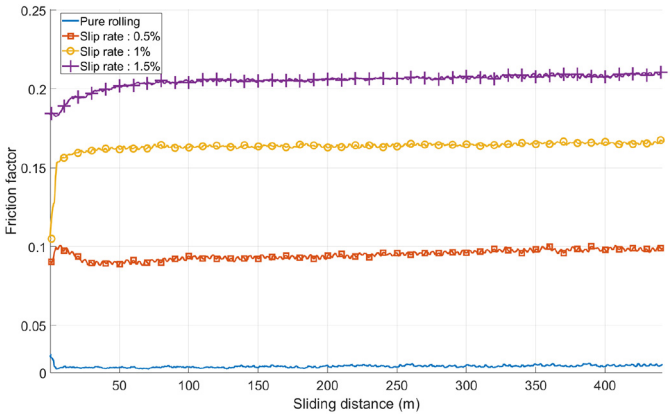

Fig. 11. Reference values of the friction factor obtained without introduction of third body in the contact on the Triboring tribometer at different slip rates.

of 54%. Test number #4 was performed in the fall with an ambient temperature of approximately 20 °C and an RH of 47%. The different curves show similar trends at the beginning and end of each test. These variations are mentioned in Section 3.1.3. The main differences resulting from the repeatability of the tests occurred in the middle of the tests and are justified here by the variations of the measured RH of approximately 7% [47%; 54%].

The shape of the curves shown in Figure 10 highlights the effect of the addition of a third external body such as autumn leaves on the adhesion of the contact studied. Indeed, for illustration purposes, the friction factor decreases over the first 100 metres travelled (on average) and then reaches its minimum. These variations reflect the accumulation of dead leaves on the surface of the disc used, creating a third body which is synonymous with a reduction in adhesion. This layer is then sheared off due to the application of a non-zero slip rate and can also undergo physico-chemical transformations mentioned in Section 1. These phenomena generate an ejection of the third formed bodies from the surface of the roller but allow to reach a maximum friction factor. In the case of Figure 10, these phenomena occur for sliding distances ranging, on average, from 100 to 470 metres. Finally, the complete ejection of the third body layer formed on the disc surface is reflected by the obtainment of a constant friction factor.

3.1.3 Adhesion tests performed without introduction of external third body

The adhesion test results without the introduction of a third body (steel-on-steel contact) at different slip rates (pure rolling, 0.5%, 1%, 1.5%) with a contact linear speed of 1.3 m/s^{-1} are presented in Figure 11. Under these conditions, the friction factor remained constant for a given slip rate, reaching a maximum value of 0.21 ± 0.02. These values of the friction factor remain globally of the same order of magnitude as a dry rail–wheel contact with sufficient slip to transmit traction and braking forces [26,27]. The increase of the friction factor with the slip rate can be explained via the bench control. The slip rate is controlled in the tribometer; therefore, the increase of this parameter imposes a motor torque proportional to the slip imposed (Eq. (1)), and consequently, a higher friction factor is required to transmit the forces. In contrast, when a slip rate of 0% is imposed on the Triboring tribometer, a close but non-zero friction factor (mean value: 0.02 ± 0.005) is obtained. This non-zero value can be explained by the fact that according to Merino [19], the slip rate is computed on the center of the elliptical contact area and is associated with measurement uncertainties ($\pm 0.02\%$ for the slip rate. Therefore, with an imposed slip rate of 0%, a near-zero yet negligible friction factor is measured.

The values of the friction factor obtained at the end of tests performed with slip rates below 1.5% (Fig. 11) were lower than 0.3, which corresponds to a reference value used in the railway industry [28,29]. These values must be compared for the same type of tribometer. For the use of a disc-on-ring tribometer, with an imposed slip rate and with a corroded disk, these values are consistent with other tests intended to study the development of rail defects caused by the white etching layer on the surface of rails [19]. This result can also be compared with the work of Zhu et al. [16,30] who found out that without the presence of an external third body, when using a pin-on-disk tribometer, the lowest values of the friction factor were obtained with a RH higher than 70% and a slip rate of 100%.

The results in Figure 11 can be compared to tests carried out using a twin disc tribometer with parts made of ER7 and R260 grade steel [25]. For all the slip rates applied in this study, the friction factors measured without the presence of dead leaves in the contact on the Triboring tribometer are lower than the data mesured from the use of a twin disc type tribometer. These differences in values could be associated with the servo laws used to maintain a constant slip rate on the Triboring Tribometer but require further investigation.

For a pure rolling condition, the low friction factor is coherent with the slip rate imposed (0%) and the near-zero tangential force measured by the contact. For an imposed slip rate higher than 0.5%, the friction factor is initially increasing, and both the tangential and normal forces reach an equilibrium for a given slip rate.

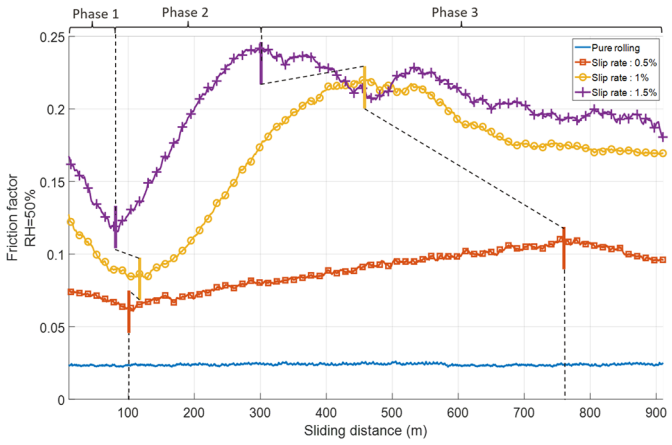

Fig. 12. Friction factor as a function of the sliding distance travelled on Triboring tribometer, plane leaves RH = 50%. Highlights of the different phases. Phase 1 extends from the beginning of the test to the point where the minimum friction factor is obtained, phase 2 extends to the point where the maximum friction factor is measured, and phase 3 extends to the point where a stabilized friction factor is obtained (corresponding to the end of a test).

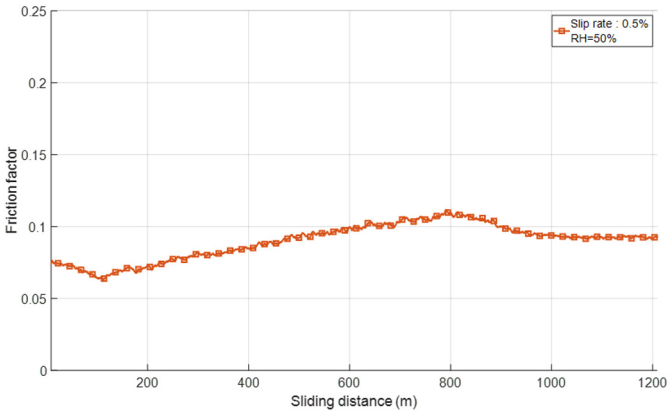

Fig. 13. Friction factor as a function of the sliding distance achieved on Triboring tribometer, plane leaves RH = 50%, slip rate : 0.5%.

3.1.4 Adhesion tests performed with an external third body introduced

Figure 12 shows the variation of the friction factor with plain leaves ingested by the contact with a RH of approximately 50% and for the same slip rates described in this section. The data obtained from a pure-rolling test with and without leaves provided an average friction factor of 0.024 ± 0.002. These low values are due to the pure-rolling conditions, associated with almost no tangential force. The increase of the imposed slip rate indicates different evolutions of the friction factor. Indeed, for the three values of imposed slip rates, the friction factor evolves according to three main phases. It decreases until reaching a minimum during the first 100 m, on average (Fig. 12 phase 1). The values obtained do not allow the transmission of all the forces in the contact. Under these slip rates, the mobilizable friction is at most equal to 0.24 in the case of a slip rate equal to 1.5%. It may also be no greater than 0.11 for a slip rate of 0.5%. The latter is below the friction factor threshold of 0.2 sufficient to allow a train to move forward [31]. This same factor increases in an almost linear progression to reach values higher than the initial ones (Fig. 12 phase 2). The maximum adhesion is reached. Finally, in the last phase, the friction factor stabilizes and tends towards a constant value (Fig. 12, phase 3).

For a slip rate of 0.5% and RH = 50%, an average stabilized friction factor equals to 0.093 was achived for a sliding distance higher than 1000 meters. The final friction factor seen on Figure 12 for a slip rate of 0.5% is equal to 0.097. This data can be seen on Figure 13. More generally, the values of friction factors visible at the end of each curve associated with different slip rates and relative humidity of the external third bodies correspond to the stabilised values associated with a full ejection of the third bodies formed onto the discs' surface.

The variations of the friction factor plotted on Figure 12 do not have the same kinetics and depend on the slip rate. At the end of the tests and for all the conditions studied, the friction factor remains on the same order of magnitude as that obtained at the end of the reference tests (Fig. 11). Similar trends were observed for other RH values (Fig. 14a, and b). Comparing the stabilized friction factor values for each of the tests at the end of phase #3 with the results of the reference tests (Fig. 11) allows one to determine whether the parts in contact were still contaminated by leaves. For a given slip rate, as the RH increases, the stabilized friction factor (i.e. at the end of each test) tends towards similar values as the references tests. These values are summarized in Figure 15.

At a constant RH, it is interesting to note that the values of the friction factor obtained at the end of the experiments increased with increasing slip rate applied on the contact.

3.2 Energy analysis and identification of wear phenomena

3.2.1 Reference energy values

The results from Figures 14a, b, and c can also be analyzed by observing the variations of the power dissipated by friction P_f (Eq. (2), Fig. 16). The variations of this quantity are used as a tool and an indicator for the comparison of the adhesion tests and the understanding of the capacity of a third body to mobilize friction through power dissipation. Indeed, linking power dissipated by friction with optical observations of the surface of the discs used during tests thus allow verification of whether the third body introduced in the contact affects the adhesion of the contact (see also Sect. 2.2). As an example and for reference, the frictional power dissipated at several slip rates and without leaves is plotted in Figure 17. Variations of P_f will then be coupled with the observation of the tribometer

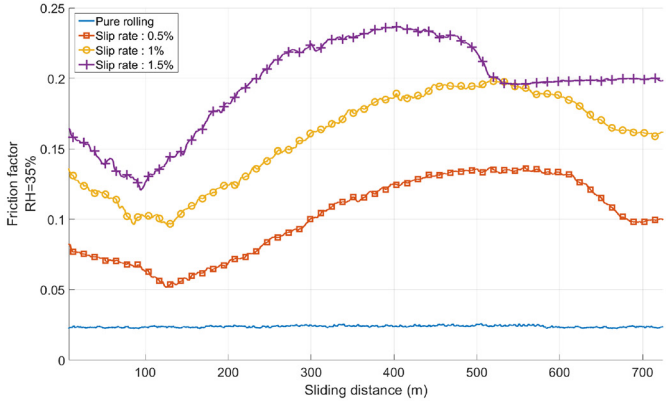

(a) friction factor, RH=35%

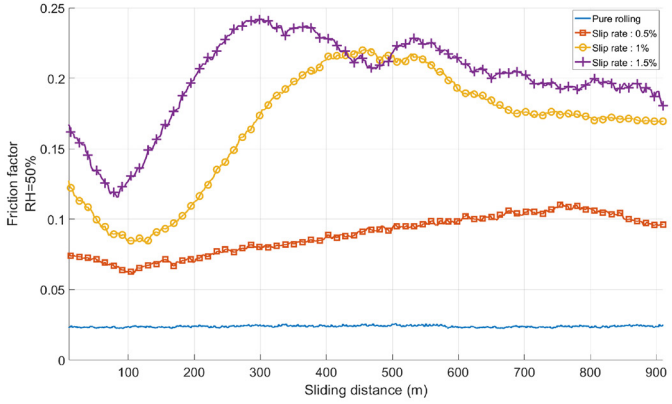

(b) friction factor, RH=50%

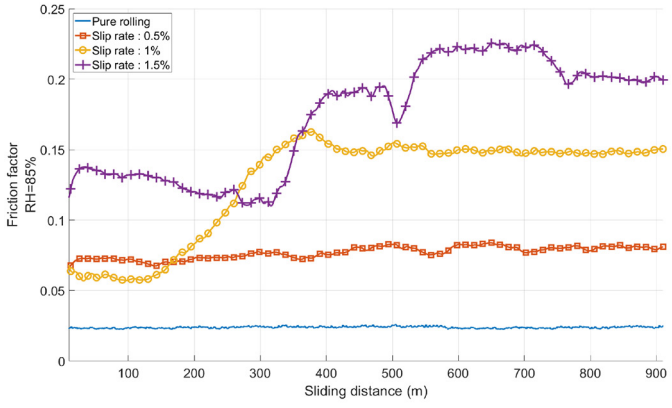

(c) friction factor, RH=85%

Fig. 14. Friction factor and RH of leaves (from tests performed in Tab. 4).

disc surface. These observations were used to characterize the morphology of the third bodies found at several moments during a test for a given RH% and slip rate.

Note: The small differences in values between the power curves given for no slip and 0.5% slip can be attributed to the similar tangential forces in these two cases. The imposed slip control of the tribometer generates tangential forces at the contact of the same order of magnitude for low slip rates such as 0% and 0.5%. The other quantities

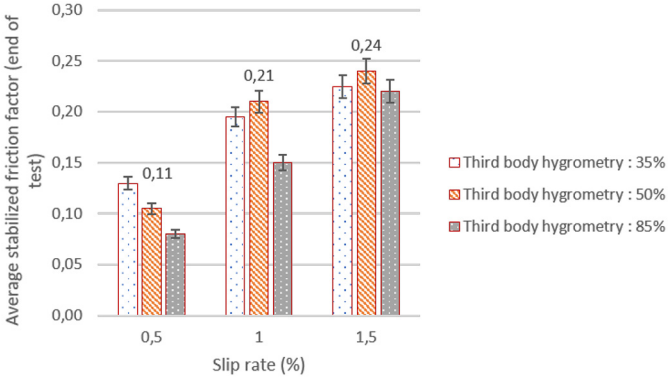

Fig. 15. Average stabilized friction factor (and standard deviation) obtained at the end of the tests performed with various slip rates and RH values of the third bodies.

(linear velocities) are for these slip rates that differ by only 1%, which also justifies these small differences in power.

3.2.2 Adhesion tests: power aspect

The data from the tests performed in Section 2.2.6 and shown in Figure 16 reveal several repeatable variations allowing five regions to be defined. One is defined when the power dissipated by friction is decreasing, constant, or increasing. The slopes plotted in Figure 18 allow the boundaries between regions ♯1 to ♯5 to be defined through the use of inflection points. An example is shown in the same figure. The different regions are explained in Section 4.1. The Section 3.2.2 aims to only present the results obtained.

Note: The test campaigns described in Table 4 were stopped at various times corresponding to stabilization of the values plotted (friction and power). The distance needed to achieve stability of the friction factor depends of the slip rate and RH applied under the test conditions. Therefore, the results presented in all the figures in this document cannot be plotted with the same horizontal axis and are cut (when able) at the closest values corresponding to time (and sliding distances) after which the measured quantities were constant. Consequently, the curves shown in Figure 16 allow the links between the difference of power dissipated by friction and adhesion through tests performed with and without leaves to be highlighted.

For pure rolling contact conditions (Figs. 16 and 17), the power dissipated by friction P_f defined by equation (2) does not include the solid deformations and the associated adhesion phenomena. Consequently, the real sliding speed measured is not zero because of these two aspects, thus justifying that the power dissipated by friction computed from the measured quantities is not nil. The equation giving Pf is thus particulary adapted to the study of the adhesion of the wheel-rail contact under rolling and sliding conditions and can thus be used to carry out the parametric study presented.

For a slip rate of 0.5%, the power dissipated by friction for all the regions only differs by less than 10% for RH values of approximately 50% and 85% when compared to a test done without leaves. In contrast, for a RH of

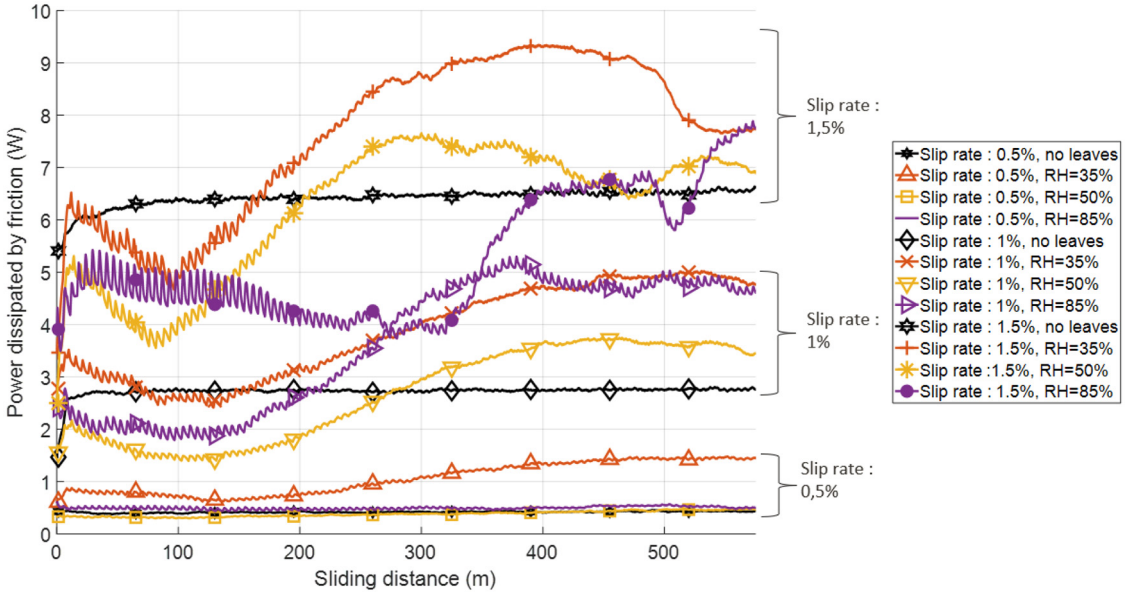

Fig. 16. Power dissipated by friction, all RH and slip rates (tests described in Tab. 4).

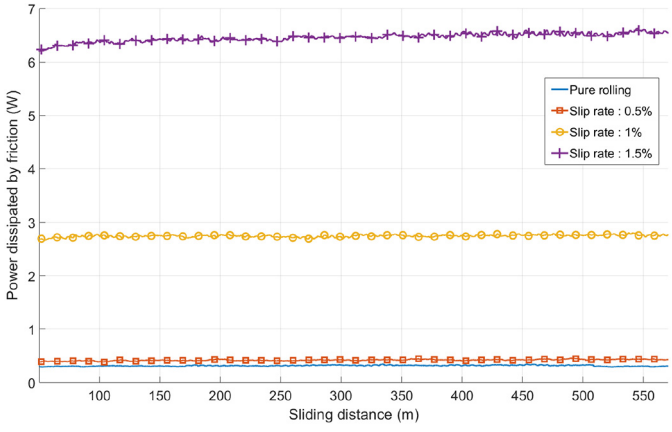

Fig. 17. Power dissipated by friction (W), reference values at different slip rates without leaves (steel-on-steel contact).

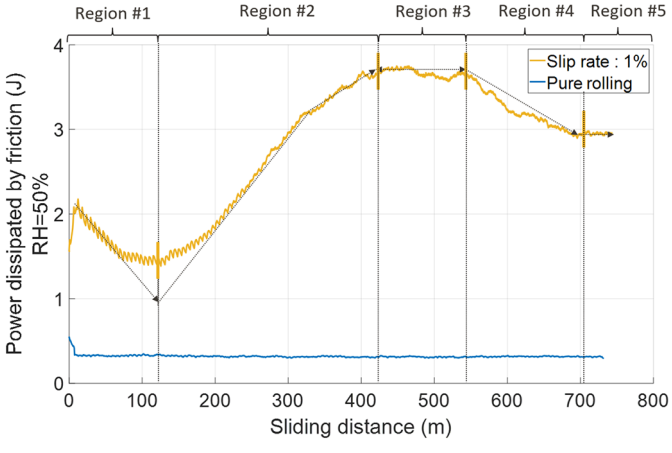

Fig. 18. Power dissipated by friction, slip rate : 1%, RH = 50%, highlight of the regions definitions.

35%, the power dissipated varies by a factor of +2 when compared to a test done without leaves in region ♯1 and by a factor of 2.6 on average in region ♯2.

For a slip rate close to 1%, the power dissipated by friction in region ♯1 decreased with RH and was lower when RH>35% than the references values (obtained with no leaves). However, in region ♯2, for all the RH values, the power dissipated by friction became higher than the references values. Moreover, RH values of both 35% and 85% tended to dissipate the same amount of power of the third body formed after region ♯2.

For a slip rate of approximately 1.5%, the power dissipated by friction was minimal and constantly lower than the references values when RH was higher than 85%. This quantity becomes maximal and higher than the reference values after region ♯2 when the RH was lower than 35%.

The power dissipated by friction data shown in Figure 16 highlights the links between RH, the slip rate, and friction variations. Indeed, as P_f reflects the physico-chemical and mechanical transformations of the third bodies obtained during the tests, the processing of the friction data through an energy quantity highlights the instantaneous capacity of the third bodies to be solicited regarding adhesion. In this case, the increase in the slip rate associated with the decrease in RH provides the greatest differences between the power dissipated by friction with or without leaves in the contact. In contrast, the decrease of the slip rate associated with a RH higher than 35% provides the lowest differences between the power dissipated by friction with or without leaves for all the regions defined. These first results translate the ability of the third body to mobilize through power dissipation friction in the contact. In these cases, a slip rate of 1% and 1.5% coupled with a RH below 35% are linked with a higher ability of the third body to increase friction in the contact. Interestingly, the main difference between a RH of leaves of 35% and 85% lies in the difference of the quantity of water initially available in the external third body

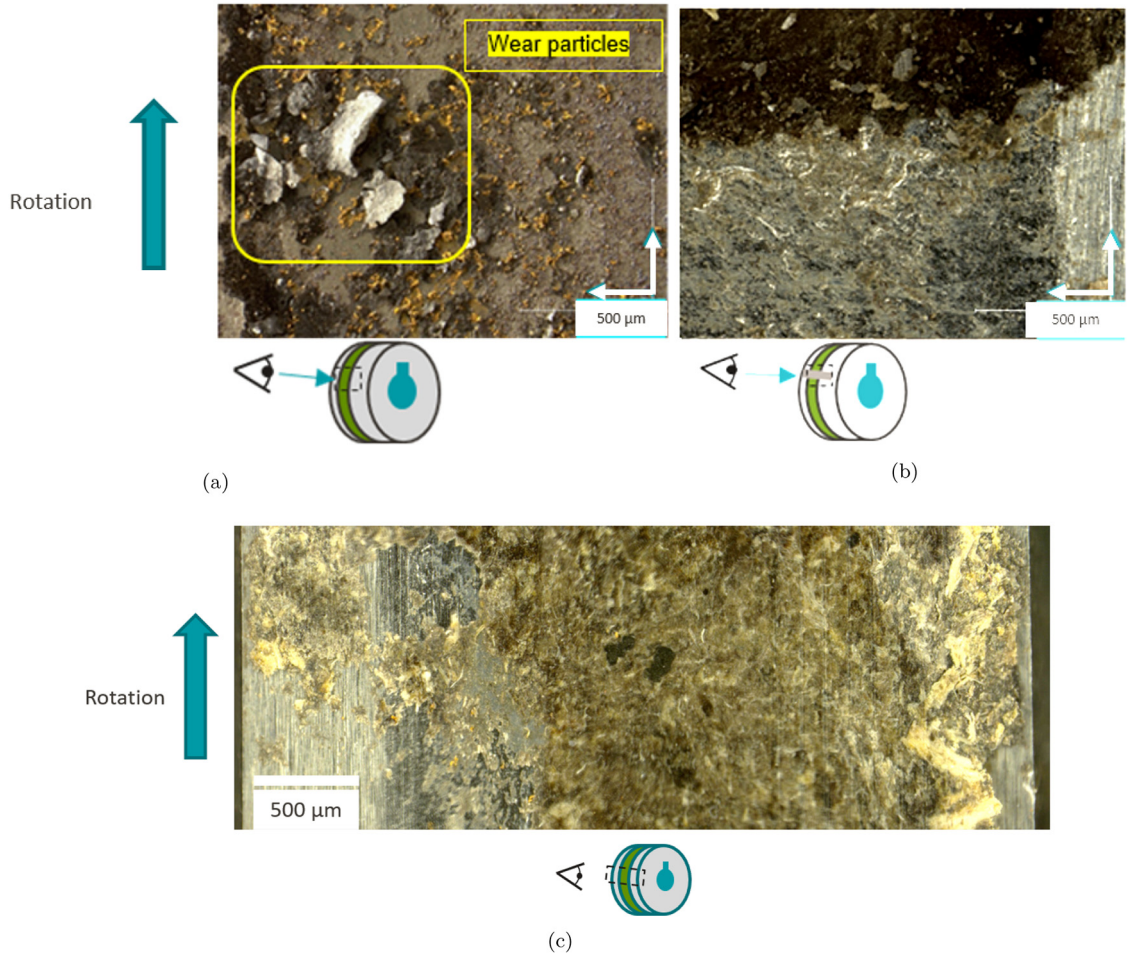

Fig. 19. Pictures of the disc surfaces after 520 m of tests, optical microscopy: slip rate 0.5%, (a) RH 35%, presence of wear debris, (b) RH 50%, intermediate case, low quantity of wear debris, thin third body thickness, (c) RH 85% presence of a third body layer of approximately 100 µm (measured through optical microscopy).

(indicated by the measure of the RH). The presence of water is one of the main components needed to activate physico-chemical reactions between organic components of leaves and steel regarding variations of adhesion in the wheel–rail contact [7,32]. Thus, reducing the amount of water found in leaves can decrease the physico-chemical effect in favor of mechanical changes of leaves under a RH below 35%.

4 Discussion

4.1 Links between power dissipated by friction and adhesion

4.1.1 Observations

The optical microscopy observation of the surface of the discs (and their third bodies) used for the tests performed with a slip rate of 0.5% allow the mechanism of adhesion reactivation for such a polluted wheel–rail contact to be explained qualitatively (see Sect. 1). Here, high adhesion levels are correlated with higher friction factors. For low-humidity levels, the third body formed, due to the increase of the frictional power dissipated, does not allow the generation of a layer of leaves with a sufficient thickness to keep the first bodies apart. The observations in Figure 19 in a low RH environment reveal the presence of wear particles reacting with a magnet. These debris are therefore from the disc and/or the ring (Fig. 19a). This result is consistent with trends observed by Lewis *et al.* [33], Zhu *et al.* [30], Rong [14] and is also found after the analysis of real third-bodies (Fig. 20) taken from the field after a wheel-slip event. The addition of a third body with a controlled RH combined with the variation of the frictional power dissipation could allow the development of a wear mechanism (wear of the first and third bodies) that increases the friction factor. In contrast, when the RH is higher than 50% (Fig. 19b and c), a third body is formed (Fig. 19c) and keeps the first bodies apart. In this case, the wheel–rail adhesion is equivalent to the adhesion of a leaf layer to the surface of a rail.

The pictures associated with the presence of several leaf layers at different relative humidities are not all black, indicating the occurrence of potential physico-chemical

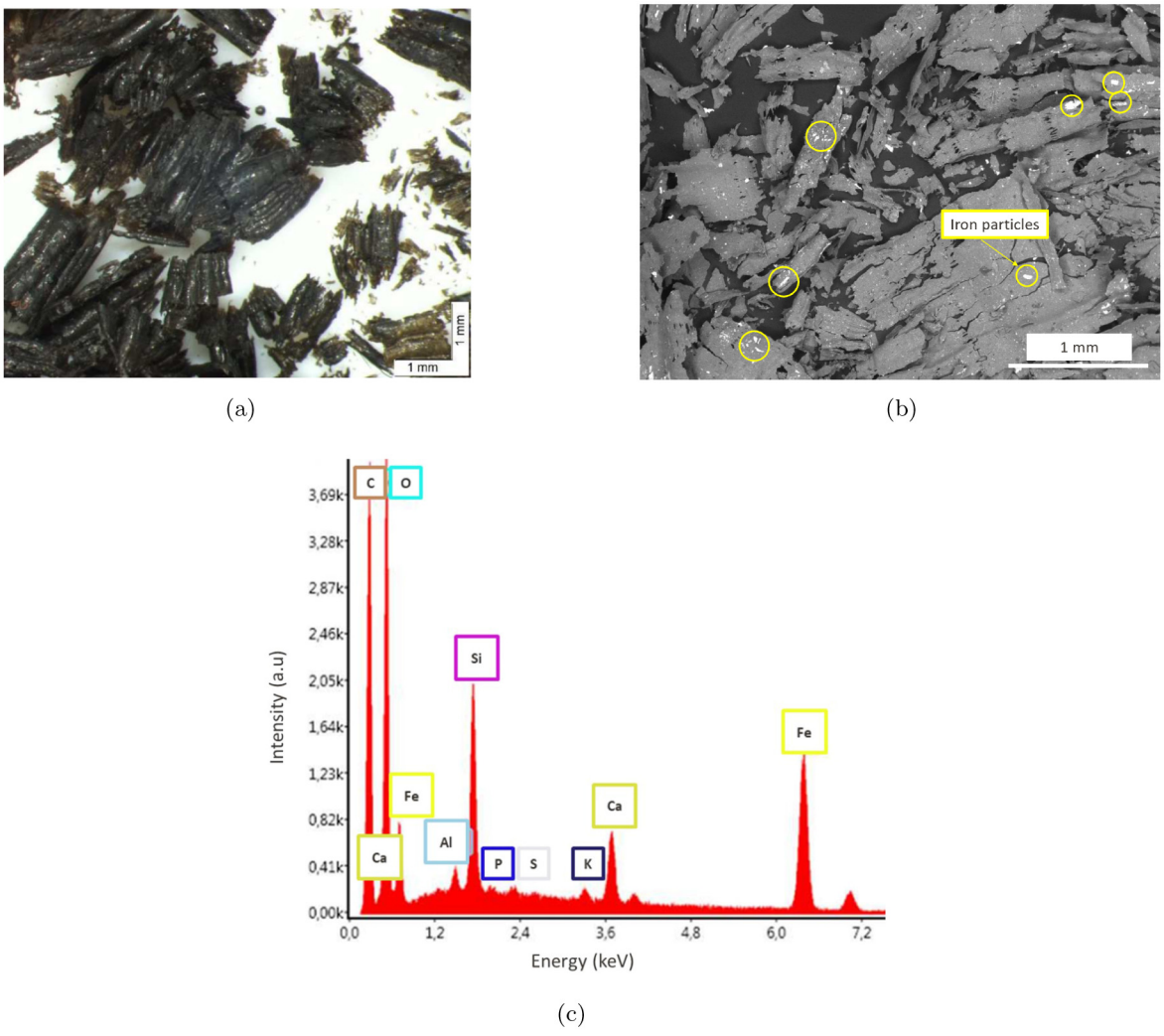

(a) (b)

(c)

Fig. 20. (a) Third-body sample taken from the field after a wheel-slip event (slip rate > 1%, optical image). (b) SEM (BSE detector, 20 kV) of the sample, (c) SEM–EDS spectrum characteristic of the sample, highlighting mineral/organic amalgam (presence of carbon, silica, and iron oxide).

reactions between the main constituents of a dead leaf's wall and its environment. These physico-chemical reactions may be related to the tannins present in the external third bodies introduced on the Triboring tribometer. This chemical compound is used in the manufacture of black and purple metallic inks [34] and was also found by Watson et al. [8] to be able by itself to reduce adhesion. Thus, the failure to obtain a black colour classically associated with an external organic third body found after an adhesion loss can be linked to physico-chemical reactions mainly involving the tannins constituting a dead leaf. This hypothesis should be verified as a further work.

The variations in power dissipated by friction plotted in Figure 16 are associated with images of the surface of an ER7 steel disc used during a test performed at a constant slip rate (1%). More generally, comparing the pictures of the disc to the dissipated power curves indicates if the adhesion losses will be linked to a mechanical aspect, a chemical one, or both. In the first case, the increase of the slip rate raises the mechanical power dissipated by friction and the shear stresses. In the second case, the chemical reactions, described by Bringel [7], Ishizaka [2], and Chen [35], allow the switch from a state where the friction factor is minimum (Fig. 21, picture a), to a state where a layer of black color described in various works [2,5,36] (see Figs. 21 and 22 pictures b and c) is formed. This layer is synonymous with the appearance of adhesion losses for the wheel–rail contact.

In Figure 22, five regions (defined when the variations of measured quantities are increasing, constant, or decreasing) can be associated with morphology of third body seen on the disc surface used for this test (Fig. 21).

Region ♯1 corresponds to the establishment of a solid film associated with the degradation of leaves due to a non-zero slip rate applied on the third body. This layer is discontinuous, homogeneous (in terms of colors, reflecting a physico-chemical stability (see also Sect. 1, in the same light and camera acquisition condition), and appears to be cohesive. However, this film was not observed on the entire surface of the ring. At this stage, the friction factor

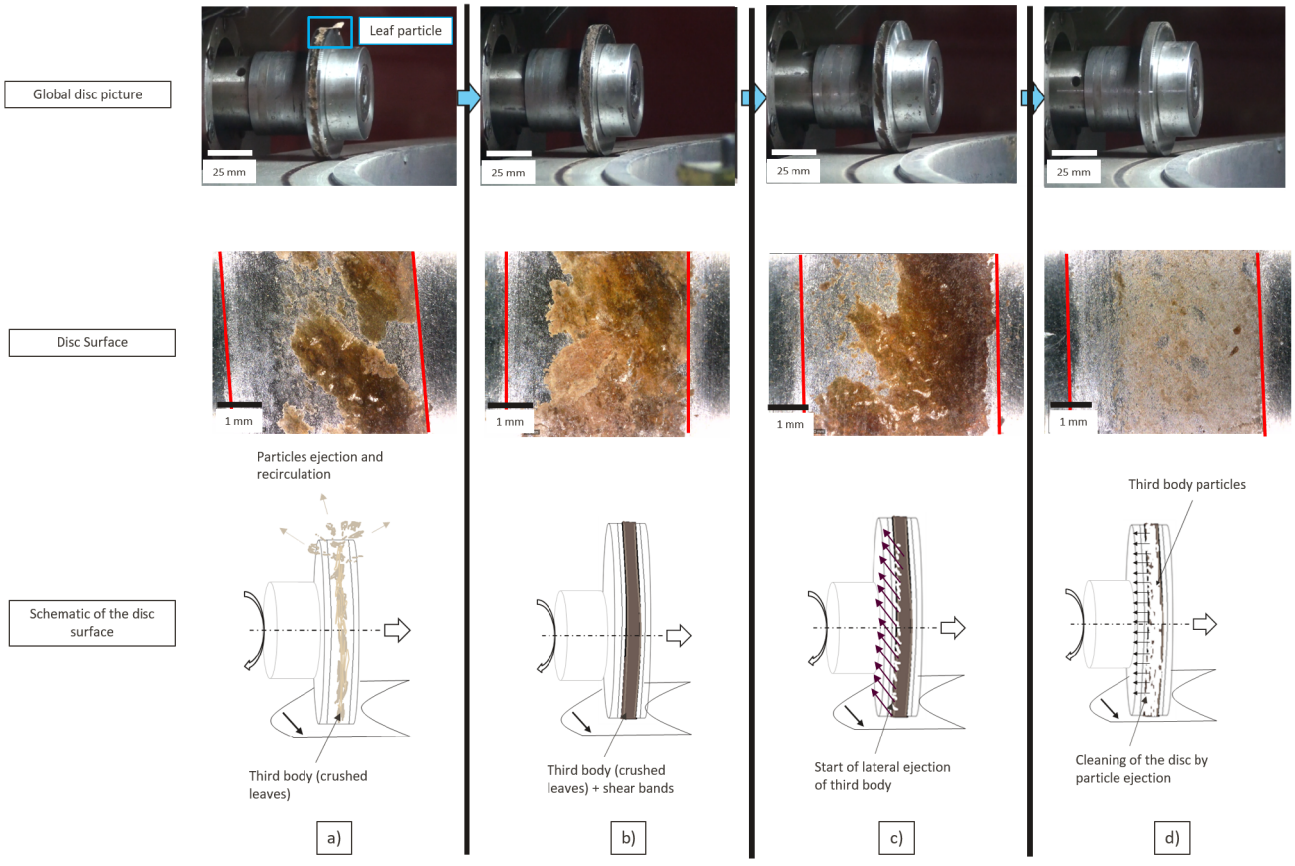

Fig. 21. Characteristic images and diagrams of the disc surface, slip rate: 1%, RH: 50%

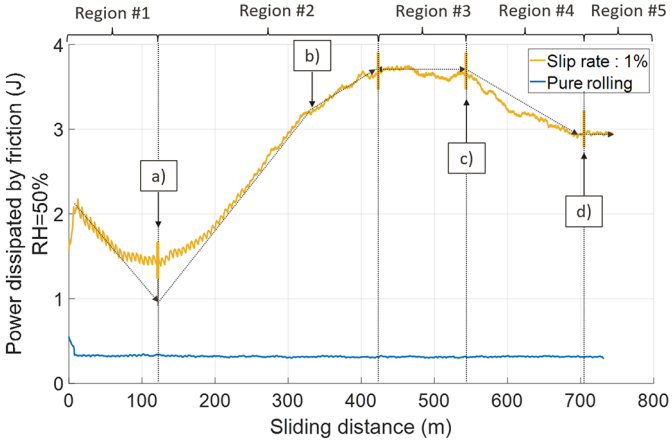

Fig. 22. Power dissipated by friction, slip rate: 1%, RH = 50%. A region is defined when the variations of the measured quantities are decreasing, constant, or increasing. The slopes plotted in this Figure define an inflection point between regions #1 and #5. Pictures of the surfaces of the disc were taken at the instants a) to d) and can be seen in Figure 21. The point a) corresponds to the minimum of adhesion reached, and points b) and c) allow the surface of the disc to be checked before and after reaching a maximum of adhesion. Point c) allows the surface of the disc used to be checked when all of the mechanical quantities are stabilized.

is under 0.1, and the capability of the contact to dissipate power by friction is minimal. This means that the capacity of a train to brake is reduced. The layer of the formed third body fails to be stable and does not stick to the disc surface. It then becomes hooked onto the disc surface and is ejected from the contact during a cycle. These variations are also reflected through the occurrence of oscillations of measured quantities, whose amplitudes are maximal in region #1 and decrease at the end of the second region.

Region ♯2 is associated with a quasi-linear increase of the friction factor associated with the beginning of a modification of the third body layer formed on the disc. The ejection of third body particles from the surface of the disc are replaced by an accumulation of third body particles. The layer formed changes of color and becomes homogeneous over the entire tread.

In **region ♯3**, the drying-up and accumulation of third-body particles enable the maximum friction factor and frictional power dissipation to be reached. This is reflected by the stabilization of the computed power dissipated by friction. It is possible to think that the presence of iron oxides on a third body particle taken at this moment and analyzed by SEM-EDS contributes (Figs. 6, 7, and Tab. 3) to the mechanical stabilization of this black colored layer (Fig. 21, b and c). The layer formed does not evolve any further from a colorimetric viewpoint in this region. It also reflects the stability of the physico-chemical reactions between the different compounds of these third

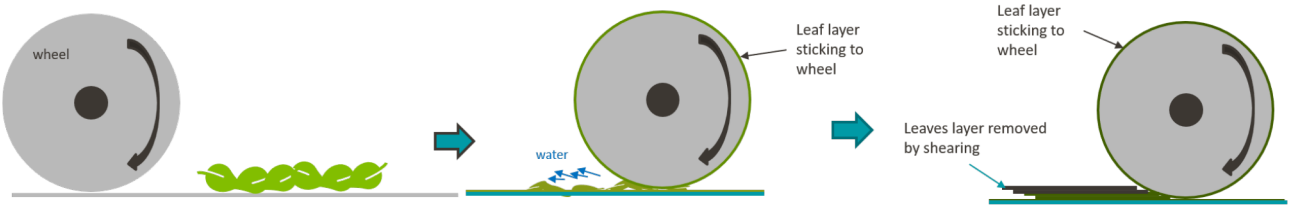

Fig. 23. Mechanism of low adhesion observed through tests using the Triboring tribometer.

bodies (see also Sect. 1). The analysis of these different regions highlights the predominant effect of the physico-chemistry linked to the transformation of the third body in **regions ♯1 to ♯3**. The color change of the third-body layer may be linked to the same chemical reactions due to the presence of water and iron oxides reacting with dead leaves. The latter were further clarified by Bringel [7] and Ishizaka [2] (mentioned in Sect. 1). In this region, all the measured quantities (friction factor, Fig. 14, and power dissipated by friction, Fig. 17) reach a maximum, decrease, and then stabilize. The sliding distance needed to achieve this stability depends of the slip rate and the RH of the external third bodies introduced in the contact. However, from the tests performed, no conclusion was drawn regarding this parameter needed to obtain a stabilized layer formed in terms of slip rate and RH.

In **region ♯4**, the formed layer was mechanically cleaned (Fig. 21 picture c), the disc surface started to regain its metallic appearance, the friction factor and the power dissipated by friction decrease linearly to reach a final plateau visible in **region ♯5** associated with image d). The predominant effect of the mechanical contact in regions ♯4 and ♯5 is demonstrated by the mechanized cleaning of the disc through the ejection of accumulated particles (Fig. 21, images d).

4.2 Effect of the morphology of leaves on adhesion losses

As mentioned in Section 3.2, the study of mechanical and energy values obtained after tests performed in Table 1 allow us to determine the conditions for which a third body is able to mobilize the friction in the contact. However, both mechanical and physico-chemical changes occur in the third body [2,7,14]. The observation of the morphology of the third bodies studied is necessary to determine and understand their characteristics at different slip rates and RH values.

RH<35%:

For a low RH (i.e., RH<35%), the structure of crushed leaves ingested through contact enables an increase of the capability of the contact to dissipate power by friction to reach a maximum value of adhesion. Initially, the low quantities of water in the stomata did not allow the third body to form a black colored layer synonymous with chemical reactions [7,37] between the wheel and rail steel. Here, it seems that the shearing of the leaf fibers allows the increase of the power dissipated by friction and the adhesion.

RH>85%:

In contrast, the presence of significant amounts of water appears to put the physico-chemical aspect of the behavior of leaves in wheel–rail adhesion at the first plane. At low slip rates (below 1%, Fig. 14), the adhesion measured at low RH is always higher than that measured at high RH.

However, the color change of the layer formed translates the occurrence of physico-chemical reactions, as explained in Section 1 and in [7,13]. We can therefore assume that the difference of power dissipated by friction at RH<35% and RH>85% is the power needed to activate the chemical reaction between lignin, cellulose, and polysaccharides (see also Sect. 1) mentioned by Bringel [7]. However, this phenomenon seems to be valid only for low slip rates ($\leq$1%). The increase of the slip rate increases the shear stresses imposed on the third body. Leaf particles are thereby shredded and ejected off the disc surface. In this case, both the mechanical aspect (associated with the increase of the shear stresses undergone by the third bodies) and physico-chemical aspects (associated with the increase of RH) appear to affect the reactivation of the adhesion, as mentioned by Ishizaka [32] and White [38].

RH$\approx$50%:

The use of leaves introduced in the contact at an ambient RH (RH$\approx$50%) allow the same levels of adhesion to be reached as those at high slip rates ($\geq$1%) and an hygrometry lower than 35%. However, the use of dead leaves with a hygrometry of approximately 50% is part of an intermediate study case. Indeed, optical and electronic observations coupled with the interpretation of experimental numerical data (forces, energies) do not make it possible to determine whether the physico-chemical reactions are predominant over the mechanical modifications of the third bodies in the evolution of the wheel–rail contact adhesion.

An assumption linked to the evacuation of the water provided during the preparation of the third bodies used is put forward here. The presence of water on the surface of a rail [39], and even when mixed with leaves [40] decreases the adhesion between a wheel and a rail. Water can be found in dew or rain and is absorbed by the stomata of a leaf (Fig. 3). The amount of water stored by them (see Figs. 23 and 24) changes locally with their RH values. Water is therefore mecanically evacuated from crushed

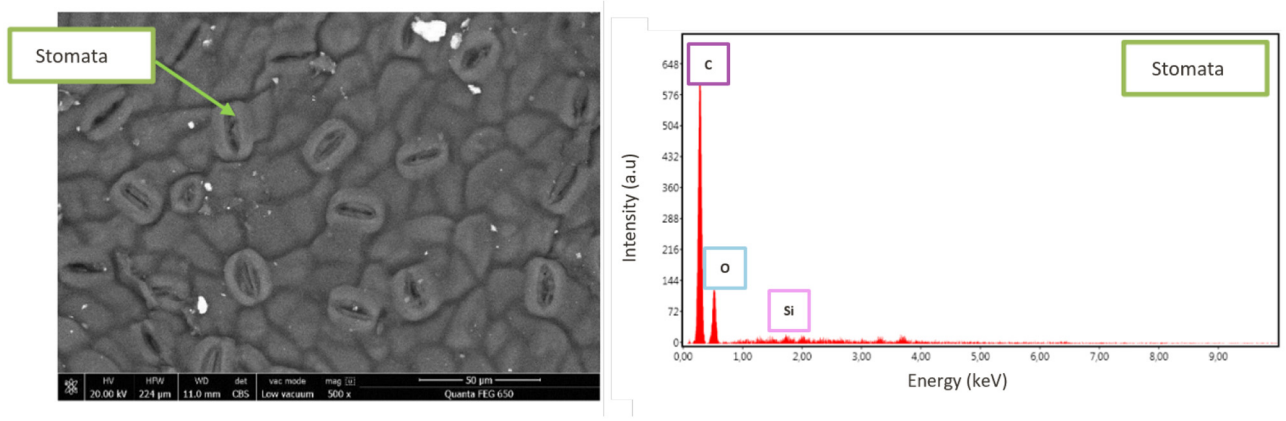

Fig. 24. SEM-EDS (BSE detector, 20 kV) image of stomata composing a leaf particle crushed by a train taken during a field survey and after tests performed under laboratory conditions.

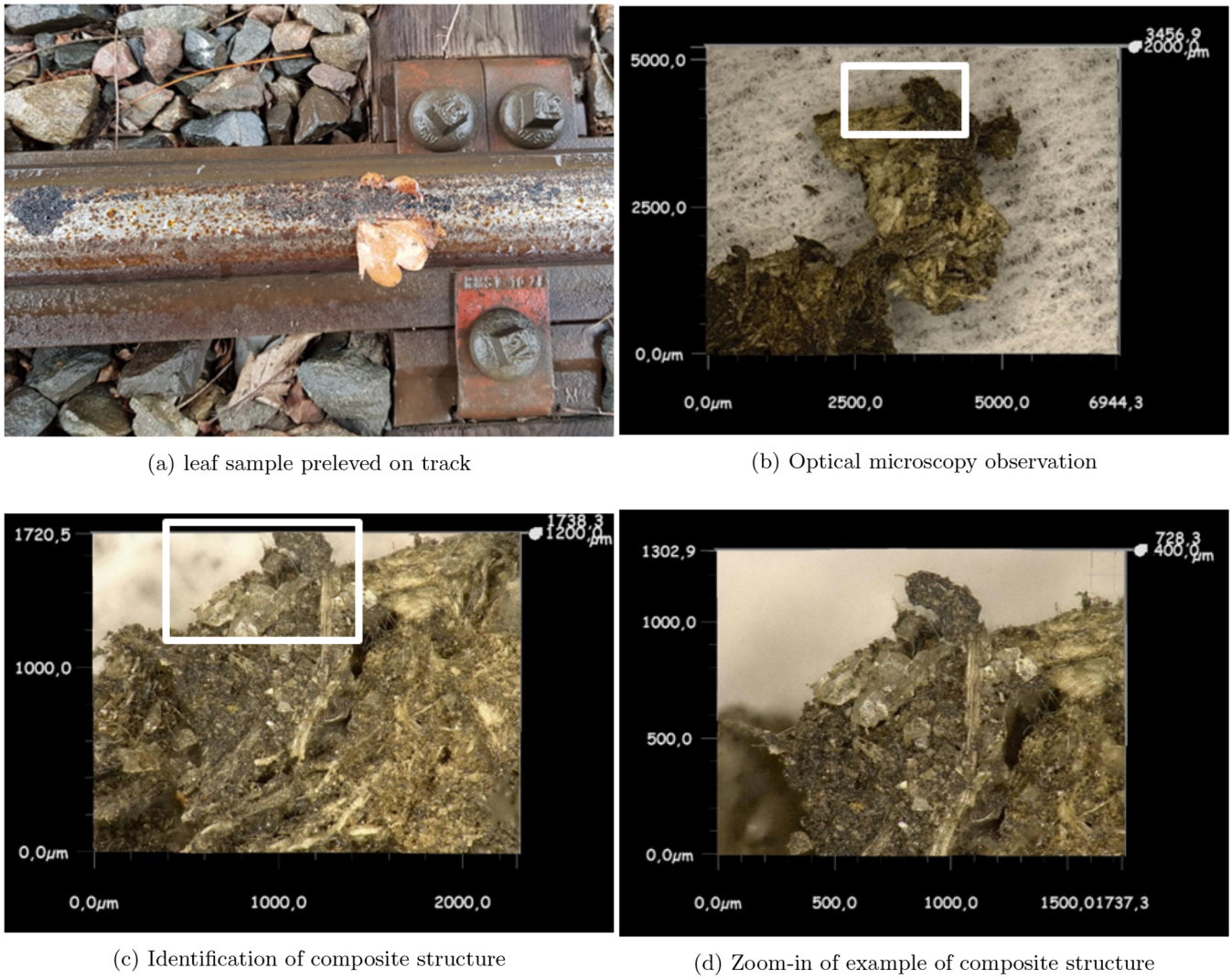

(a) leaf sample preleved on track

(b) Optical microscopy observation

(c) Identification of composite structure

(d) Zoom-in of example of composite structure

Fig. 25. Emphasis on the composite structure of the third bodies collected on the tracks. The white rectangles correspond to the areas observed at different magnifications.

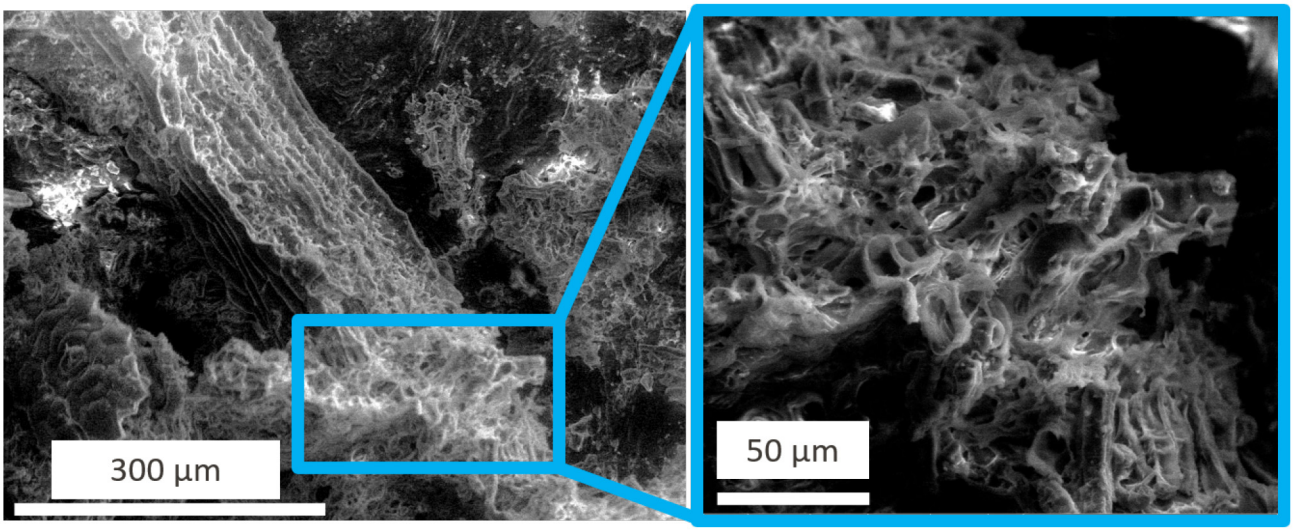

Fig. 26. Evidence obtained through SEM observation (SE detector, 15 kV) of a sponge-like structure (with porosities) of a third body collected during a test (RH = 85%, slip rate: 0.5%).

leaves onto a rail surface. The stomata (Figs. 3 and 7) are then crushed and are no longer visible by optical or electronic observation of the third bodies studied (Figs. 6 and 24).

Specifically, when third bodies composed of leaves are compressed under Hertzian pressures of approximately 1 GPa (see Sect. 1), the water present in the stomata of leaves is mechanically ejected from the contact. The structures of the leaf fibers are consequently modified. Various observations of third body samples during field operations and laboratory experiments have allowed the composite structure (fiber and matrix) to be highlighted (Fig. 25). After entering the contact, the fiber components mix with the plant matrix of the dead leaf body and generate a sponge-like structure that is able to retain a small amount of water (Figs. 25b-d). These structures were highlighted by SEM observations (Fig. 26). It can therefore be assumed that the increase in the slip rate accelerates the mechanical degradation through the shearing of the plant fibers. Their ability to retain the stored water decreases ([2,30], Fig. 23). The increase of the slip rate can also therefore increase the kinetics of the chemical reactions related to the degradation of the leaves. The power dissipated by friction in the contact thus modifies the nature of the third body formed and can serve as a catalyst for the physico-chemical transformations occurring in the third bodies formed.

5 Conclusion

The effect of the hygrometry rate of an external third body introduced into the contact reproduced on a disc-on-ring tribometer with a constant slip rate was investigated. This type of geometry is very similar to that of the tribological circuits of a wheel–rail contact. The use of mechanical quantities (friction factor, power dissipated by friction) associated with the observation of the surfaces of the first bodies highlighted the repeatable and modulable phenomena. The analysis of the third bodies by optical and electronic observation allowed the authors to compare their morphologies obtained under laboratory conditions and after field sampling.

The elements mentioned in this article enable the highlight of the fact that the adhesion of a wheel-rail contact with fallen leaves is strongly influenced by the slip rate applied to the contact as well as by the relative humidity of the third organic bodies. These two parameters are related to variations of the contact's adhesion which are associated with mechanical and physico-chemical phenomena. Thus, from an industrial pointview, the results of this study could be used to initiate discussions on the application of slip rate control laws associated with the operation of trains, since the latter can increase or reduce the distances linked to a train adhesion loss. The work mentioned in this article has also shown the influence of the relative humidity of the external third bodies on the adhesion of a rail-wheel contact. Thus, today, this work can benefit the railway industry by showing different variations in railway adhesion for specific humidity conditions. This data can be taken into account for the development of methods and tools to alter the relative humidity of third organic bodies in order to mitigate the loss of adhesion of a train to its rails.

More generally, the authors observed:

- Variations in the hygrometry of the third bodies coupled with changes of the slip rate have a significant effect on the variations of adhesion in a wheel–rail contact. Low RH values and high slip values ($<$1.5%) provide sufficient available adhesion levels for achieving safe train movements.
- Decreasing RH increases the generation of wear debris from the first bodies, but allows the highest levels of available adhesion to be achieved.
- Increasing RH causes the creation of a third-body layer, which decreases the available adhesion but

reduces the generation of wear debris. This condition is unfavorable for obtaining sufficient available adhesion for a train to run.
– Increasing the slip rate of the contact increases the ability of the third body to dissipate energy throughout the contact compared with testing without the introduction of an external third body. In this case, with leaf pollution, the adhesion of a train can be higher than for one in a dry contact but only after several meters of rolling.

Conflict of interest

The authors declare that they have no known competing financial interests or personal relationships that could have appeared to influence the work reported in this paper.

Acknowledgements The authors would like to thank the French National Railway Society and the Association Nationale de la Recherche et de la Technologie (ANRT) for financial support; P. Veuillet and A. Pâquet (INSA-Lyon,LaMCoS) for their technical support during the mounting of the bench and the realization of the tests; and R. Gadiou and O. Bringel (Université de Haute-Alsace, UHA-IS2M) for their support regarding the analysis of the tests.

References

[1] B. White, R. Nilsson, U. Olofsson, A. Arnall, M. Evans, T. Armitage, J. Fisk, D. Fletcher, R. Lewis, Effect of the presence of moisture at the wheel–rail interface during dew and damp conditions, Proc. Inst. Mech. Eng. F **232**, 979–989 (2018)
[2] K. Ishizaka, S.R. Lewis, R. Lewis, The low adhesion problem due to leaf contamination in the wheel/rail contact: bonding and low adhesion mechanisms, Wear **378–379**, 183–197 (2017)
[3] M. Godet, The third-body approach: a mechanical view of wear, Wear **100**, 437–452 (1984)
[4] Y. Berthier, Mécanismes et tribologie. PhD thesis (1988)
[5] P.M. Cann, The "leaves on the line" problem-a study of leaf residue film formation and lubricity under laboratory test conditions, Tribol. Lett. **24**, 151–158 (2006)
[6] E. Konomics, Description of a plant stomata (2012)
[7] O. Bringel, Etude des caractéristiques chimiques et structurales, d'une pollution solide, formée sur les rails de voies ferrées et les roues de matériels roulants et ayant un caractère isolant (d'un point de vue électrique). PhD thesis (2021)
[8] M. Watson, B. White, J. Lanigan, T. Slatter, R. Lewis, The composition and friction-reducing properties of leaf layers: leaf layer friction and composition, Proc. Roy. Soc. A: Math. Phys. Eng. Sci. **476** (2020)
[9] K. Ishizaka, S.R. Lewis, D. Hammond, R. Lewis, Chemistry of black leaf films synthesised using rail steels and their influence on the low friction mechanism, RSC Adv. **8**, 32506–32521 (2018)
[10] J.D. Hem, Complexes of ferrous iron with tannic acid, Chem. Iron Natural Water **1459**, 75–94 (1960)
[11] W. Skipper, A. Chalisey, R. Lewis, A review of railway sanding system research: wheel/rail isolation, damage, and particle application, Proc. Inst. Mech. Eng. F **234**, 567–583 (2020)
[12] P. Merino, S. Cazottes, V. Lafilé, M. Risbet, A. Saulot, S. Bouvier, J. Marteau, Y. Berthier, How to reproduce a mechanical white etching layer (WEL) on rail surface thanks to a new experimental wheel-rail contact test bench, Wear **482–483** (2021)
[13] K. Ishizaka, B. White, M. Watson, S.R. Lewis, R. Lewis, Influence of temperature on adhesion coefficient and bonding strength of leaf films: a twin disc study, Wear **454–455**, 203330 (2020)
[14] K. Jie Rong, Y. Long Xiao, M. Xue Shen, H. Ping Zhao, W.J. Wang, G. Yao Xiong, Influence of ambient humidity on the adhesion and damage behavior of wheel–rail interface under hot weather condition, Wear **486–487**, 204091 (2021)
[15] D.T. Eadie, H. Harrison, R. Kempka, R. Lewis, A. Keylin, N. Wilson, Field assessment of friction and creepage with a new tribometer, in Proceedings of the 11th International Conference on Contact Mechanics and Wear of Rail/wheel Systems, CM 2018 (2018), pp. 208–217
[16] Y. Zhu, Y. Lyu, U. Olofsson, Mapping the friction between railway wheels and rails focusing on environmental conditions, Wear **324–325**, 122–128 (2015).
[17] U. Olofsson, K. Sundvall, Influence of leaf, humidity and applied lubrication on friction in the wheel-rail contact: Pin-on-disc experiments, Proc. Inst. Mech. Eng. F **218**, 235–242 (2004)
[18] British Steel, Rail Steel Grades - Steel Compositions and Properties (2017)
[19] P. Merino, Reproduction experimentale du contact roue-rail à échelle réduite. PhD thesis, INSA Lyon (2019)
[20] AFNOR, NF EN 13262+A2, applications ferroviaires, essieux montés et bogies, roues - prescription pour le produit (2011)
[21] S. Simon, A. Saulot, C. Dayot, X. Quost, Y. Berthier, Tribological characterization of rail squat defects, Wear **297**, 926–942 (2013)
[22] B. White, R. Lewis, Simulation and understanding the wet-rail phenomenon using twin disc testing, Tribol. Int. **136**, 475–486 (2019)
[23] A. Meierhofer, C. Hardwick, R. Lewis, K. Six, P. Dietmaier, Third body layer-experimental results and a model describing its influence on the traction coefficient, Wear **314**, 148–154 (2014)
[24] K. Ishizaka, The Low Adhesion Problem due to Leaf Contamination in the Wheel/Rail Contact : Bonding and Low Adhesion Mechanisms. PhD thesis, The university of Sheffield (2019)
[25] E. Gallardo-Hernandez, R. Lewis, Twin disc assessment of wheel/rail adhesion, Wear **265**, 1309–1316 (2008)
[26] R. Lewis, U. Olofsson, Basic tribology of the wheel–rail contact, in Wheel–Rail Interface Handbook (Elsevier, 2009), pp. 34–57
[27] C.R. Fulford, Review of Low Adhesion Research. RSSB report CRF04002, 2004
[28] C.T. Foo, B. Omar, A.S. Jalil, A review on recent wheel/rail interface friction management, J. Phys.: Conf. Ser. **1049**, 012009 (2018)
[29] K. Ishizaka, S.R. Lewis, D. Hammond, R. Lewis, Chemistry of black leaf films synthesised using rail steels and

their influence on the low friction mechanism, RSC Adv. **8**, 32506–32521 (2018)
[30] Y. Zhu, U. Olofsson, H. Chen, Friction between wheel and rail: a pin-on-disc study of environmental conditions and iron oxides, Tribol. Lett. **52**, 327–339 (2013)
[31] C.R. Fulford, Review of Low Adhesion Research. RSSB report CRF04002 (2004)
[32] K. Ishizaka, B. White, M. Watson, S.R. Lewis, R. Lewis, Influence of temperature on adhesion coefficient and bonding strength of leaf films: a twin disc study, Wear **454–455**, 203330 (2020)
[33] S.R. Lewis, R. Lewis, U. Olofsson, D.T. Eadie, J. Cotter, X. Lu, Effect of humidity, temperature and railhead contamination on the performance of friction modifiers: Pin-on-disk study, Proc. Inst. Mech. Eng. F **227**, 115–127 (2013)
[34] D. Diringer, The Book Before Printing: Ancient, Medieval and Oriental (1982)
[35] H. Chen, T. Ban, M. Ishida, T. Nakahara, Experimental investigation of influential factors on adhesion between wheel and rail under wet conditions, Wear **265**, 1504–1511 (2008)
[36] S.R. Lewis, R. Lewis, J. Cotter, X. Lu, D.T. Eadie, A new method for the assessment of traction enhancers and the generation of organic layers in a twin-disc machine, Wear **366–367**, 258–267 (2016)
[37] E. Kontturi, T. Vuorinen, Indirect evidence of supramolecular changes within cellulose microfibrils of chemical pulp fibers upon drying, Cellulose **16**, 65–74 (2009)
[38] B. White, Using Tribo-Chemistry Analysis to Understand Low Adhesion in the Wheel-Rail Contact. PhD thesis, The University of Sheffield (April 2018)
[39] W.J. Wang, H.F. Zhang, H.Y. Wang, Q.Y. Liu, M.H. Zhu, Study on the adhesion behavior of wheel/rail under oil, water and sanding conditions, Wear **271**, 2693–2698 (2011)
[40] R. Lewis, E.A. Gallardo-Hernandez, T. Hilton, T. Armitage, Effect of oil and water mixtures on adhesion in the wheel/rail contact, Proc. Inst. Mech. Eng. F **223**, 275–283 (2009)

Cite this article as: S. Guidoum, P. Merino, A. Saulot, Y. Berthier and S. Hervieu, Experimental study of the influence of the relative humidity of leaves and their link to adhesion losses in the wheel-rail contact, Mechanics & Industry **23**, 23 (2022)